12

Testing of Aspheric Wavefronts and Surfaces

D. Malacara, J. C. Wyant, K. Creath, and J. Schmit

12.1. INTRODUCTION

Aspheric wavefronts with spherical aberration are produced by optical systems using spherical as well as aspherical surfaces. Aspheric surfaces are used in optical systems in order to improve aberration correction and, frequently, to decrease the number of optical elements needed to make this correction satisfactorily. However, if these surfaces are tested while being isolated from the rest of the optical system to which they belong, they frequently produce aspherical wavefronts. The interferometric testing and measurement of aspherical wavefronts are not as simple as in the case of spherical or flat wavefronts.

To test aspherics, often a null test is issued. The usual definition of a null test is that which produces a fringe-free field when the desired wavefront is obtained. Then, if a tilt between the wavefront under test and the reference wavefront is added and the paraxial curvature of them are equal, straight and parallel fringes are obtained. Under these conditions, any deviation from straightness of the fringes is a graphical representation of the wavefront deformation. This is the ideal testing procedure because the desired wavefront is easily identified and measured with high accuracy. There are several methods to obtain this null test, but sometimes this is not simple and may even be a source of possible errors.

Typically, if a quantitative retrieval of the wavefront is desired, the interferogram is imaged onto a CCD detector. Then, the straightness of the fringes for a perfect wavefront is useful but not absolutely necessary. However, the minimum fringe spacing should be larger than twice the pixel size in the detector. This is the well-known Nyquist condition, which may be impossible to satisfy if the wavefront has a strong asphericity.

In a Fizeau or Twyman–Green interferogram, a strong rotationally symmetric aspheric wavefront has many fringes when taken at the paraxial focus setting as shown in Figure 12.1(a). By adding a small curvature to the wavefront, that is, by adding defocusing, the minimum fringe spacing can be slightly reduced. For

Optical Shop Testing, Third Edition Edited by Daniel Malacara

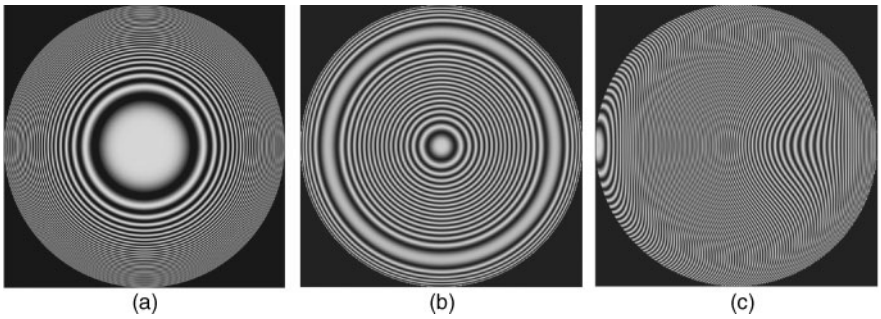

FIGURE 12.1. Interferogram of an aspheric wavefront with primary spherical aberration (a) at the paraxial focus, without tilt; (b) at the best focus, without tilt; and (c) at the best focus, with large tilt.

example, let us assume that the aspheric wavefront with rotational symmetry can be represented by

$$W(S) = aS^2 + bS^4 \tag{12.1}$$

where S is the radial distance from the optical axis ($S^2 = x^2 + y^2$), the first term to the right of the equal sign is the defocusing, and the second term is the asphericity (primary aberration). The defocusing coefficient a should be chosen so that the minimum fringe spacing on the pupil aperture is as large as possible. The fringe spacing is defined by the wavefront slope, so the maximum wavefront slope has to be minimized. This condition is satisfied if (see Fig. 12.2)

$$a = -\frac{3}{2} b S_{\max}^2 \tag{12.2}$$

This increases the minimum fringe spacing in the interferogram by a factor of 4, as illustrated in Figure 12.1(b).

To simplify the analysis of a single fringe pattern with closed fringes, it is sometimes necessary to introduce a large tilt so that only open fringes appear as shown in Figure 12.1(c). Then, we say that a linear carrier has been introduced along

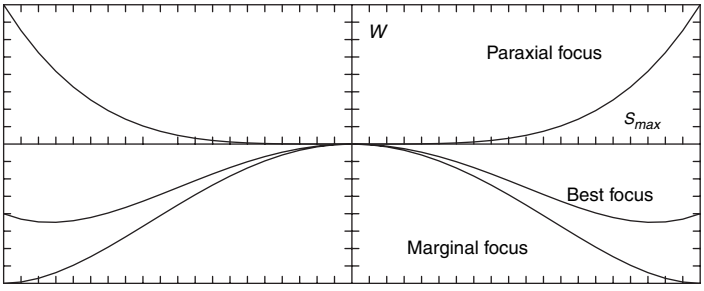

FIGURE 12.2. Wavefront profiles for primary spherical aberration at three different focus settings.

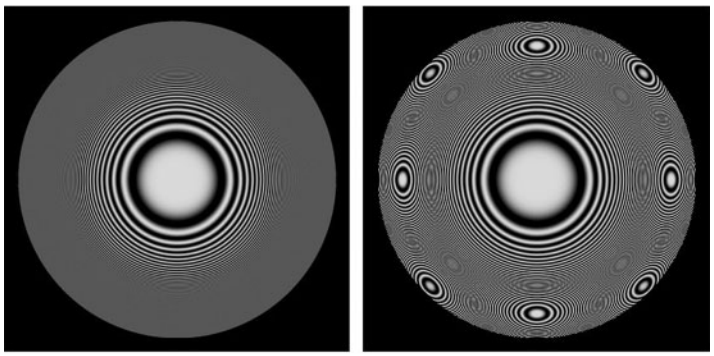

FIGURE 12.3. Interferogram of an aspheric wavefront with primary spherical aberration (a) at the paraxial focus, without tilt; (b) at the best focus, without tilt; and (c) at the best focus, with large tilt.

the x axis. With these conditions, when scanning the wavefront along horizontal lines the same fringe is not scanned twice. The problem with this method is that the introduction of the large tilt that opens the fringes also decreases the fringe spacing. The minimum fringe spacing occurs where the sum of the slope of the wavefront under test plus the slope of the reference wavefront tilt is the largest.

In a rotationally symmetric aspheric wavefront, the fringes are concentric rings and also in many other interferograms the fringes may close, forming loops. This kind of interferograms are difficult to analyze and frequently some special complicated techniques have to be used. A second and more important disadvantage is that the fringe spacing is quite small near the edge of the pupil.

When sampling an interferogram where the Nyquist condition is violated, each pupil detector measures the average intensity of the light falling over its small area. If the fringe spacing is smaller than twice the pixel size, the image of the fringes is washed out or the contrast will be greatly reduced if these two dimensions are similar as shown in Figure 12.3(a). If the pixel size is much smaller than its spacing, instead of a low fringe contrast, some false spurious fringes will appear, as shown in Figure 12.3(b). This effect is known as aliasing. Most CCD detectors have a pixel spacing almost equal to the pixel size. So, fringe aliasing is not common.

12.2. SOME METHODS TO TEST ASPHERIC WAVEFRONTS

There are several methods that had been used to test aspheric surfaces, which will be described in this chapter. The methods for testing the quality of aspheric surfaces that have been developed can be classified into the following categories:

1. One of the several possible non-null classic tests can be quantitatively used, measuring the wavefront with the Foucault, Ronchi or Hartmann tests, mathematically

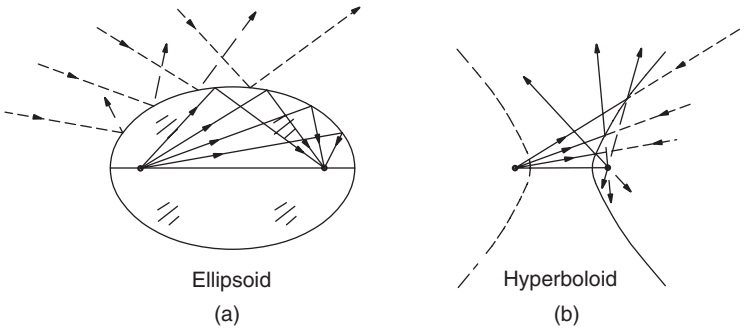

FIGURE 12.4. Reflective concave and convex ellipsoidal and hyperboloidal surfaces.

in calculating the surface deformations with respect to the closest sphere. This process in general is time consuming, and frequently the accuracy of the results is not high enough if the aspheric deformation is strong, due to their relatively smaller sensitivity as compared with interferometry. These methods are described in Chapters 8–10.

2. For conicoidal surfaces with symmetry of revolution, there is always a pair of conjugate focii that are free of spherical aberration as illustrated in Figure 12.4. Then, if the surface under test is illuminated with a convergent or divergent wavefront with the center of curvature at the proper focus, the reflected wavefront is spherical and thus is easier to test. To produce the necessary illuminating wavefront, some auxiliary optical elements are nearly always necessary. There are several of these null configurations that will be described here.

3. Some additional optical elements can be added to the testing system to compensate for the spherical aberration of the wavefront reflected from the aspheric surface. Then, an auxiliary optical system is designed so that, in combination with the aspheric surface, it forms a stigmatic image of a point source. The auxiliary optical system is called a null corrector or null compensator. These methods will be described in this chapter.

4. If only one interferogram picture is taken and the asphericity is not very strong, several interferometric methods can be used to evaluate the fringe pattern. However, if the asphericity is strong and the fringe spacing is not larger than twice the pixel separation at the detector (Nyquist condition), the interferogram may become impossible to analyze. Analysis is possible only with a procedure described by Greivenkamp (1987) and only when the following conditions are satisfied:

(a) The pixel size is smaller than the pixel separation. Then, spurious fringes will appear where the Nyquist condition is not satisfied.

(b) The wavefront's general shape is known.

(c) The expected wavefront is smooth. The problem is then solved by proper phase unwrapping until the retrieved wavefront and its slopes are continuous.

5. With phase-shifting techniques, a series of Fizeau or Twyman–Green interferogram can be used without the introduction of tilt, even if closed loop fringes are formed. A series of a minimum of three interferograms have to be taken with different values of the constant term for the phase, also called piston term. Then, the interpretation of the wavefront evaluation becomes relatively simple from a mathematical point of view, but it is much more complicated from the experimental point of view. The phase shifting techniques are described in detail in Chapter 14. When measuring an aspheric wavefront with phase shifting, the defocusing term has to be properly chosen so that the fringe spacing is minimum as described before. As pointed out before, the limitation is that by using the optimum focus setting, the Nyquist condition is not violated.

6. If the wavefront has a strong deviation from sphericity, even phase shifting techniques become impossible. Another possibility under these conditions is to test the wavefront by dividing the complete aperture into small regions where the Nyquist condition is not violated. In other words, in all small regions the fringe spacing should be larger than twice the pixel separation. This technique, sometimes referred to as a wavefront stitching technique, will be described in this chapter.

7. If a longer wavelength is used, the dynamic range is increased by reducing some of its sensitivity. For example, by operating at 10.6 μm, the dynamic range is increased twenty times, approximately.

8. Sources and detectors for longer wavelengths may be prohibitively expensive. A solution to this problem may be found in two-wavelength methods, where fringes at longer (synthetic) wavelength are created by simultaneous exposure at two different wavelengths. These fringes, which are resolvable for high slopes at a longer wavelength, may be analyzed with a phase shifting method. Different synthetic wavelengths can be obtained by combining different visible wavelengths, as described in Chapter 15 and Section 12.13 in this chapter.

9. Lateral or radial shear interferometry, as described in Chapters 4 and 5, provides a larger dynamic range for testing strong aspherics, but a smaller sensitivity.

12.3. IMAGING OF THE INTERFERENCE PATTERN IN NON-NULL TESTS

An aberrated wavefront continuously changes its shape as it travels; therefore, if the wavefront is aspherical, the interference pattern will also continuously change as the beam advances as shown in Figure 12.5. Since the errors of an instrument are represented by wavefront distortions on the pupil, the interferogram should represent the wavefront deformations at that place.

The problem is even worse if the wavefront travels twice through the optical system during the test. For example, when testing a lens with any of the configurations as described in Chapter 2, the wavefront travels twice through the lens; the second time, it travels after being reflected from the small mirror in front of the lens. If the aberration is small, the total wavefront deformation is twice the deformation

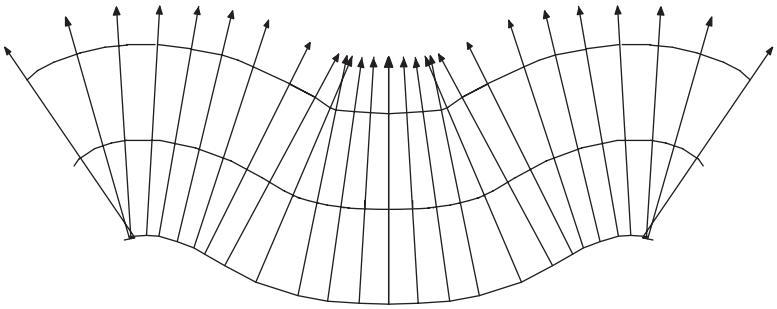

FIGURE 12.5. Change in the wavefront profile as it travels.

introduced in a single pass through the lens. However, if the aberration is large, this condition is not followed, because the wavefront changes while traveling from the lens to the mirror and back to the lens. Then, the spot in the surface on which the defect is located is not imaged back onto itself by the concave or convex mirror, and the ray will not pass through this defect the second time. Great confusion then results with regard to the interpretation of the interferogram, since the defect is not precisely duplicated by the double pass through the lens.

It may be shown that the image of the lens is formed at a distance L from the lens, which is given by

$$L = \frac{2(F-r)^2}{2F-r} \tag{12.3}$$

where F is the focal length and r is the mirror radius of curvature ($r > 0$ for a convex mirror and $r < 0$ for a concave mirror). We may see that the ideal mirror is convex and very close to the lens ($r \sim F$).

An adequate optical arrangement has to be used if the lens under test has a large aberration, in order to image its pupil back on itself. Any auxiliary lenses or mirrors must preserve the wavefront shape. Some examples of these arrangements are shown in Figure 12.6 (Malacara and Menchaca, 1985).

However, for microscope objectives these solution is not satisfactory because the ideal place to observe the fringes is at the back focus. In this case the Dyson (1959) system illustrated in Figure 12.7 is an ideal solution. It is interesting to point out that Dyson's system may be used to place the self-conjugate plane at concave or convex surface, while maintaining the concentricity of the surfaces.

Even if the wavefront passes only once through the optical system under test, the second problem is to image the interference pattern on the observing detector, screen, or photographic plate. The imaging lens does not need to preserve the wavefront shape if it is placed after the beam splitter, and thus both interfering wavefronts pass through this lens. However, this lens has to be designed in such a way that the interference pattern is imaged without any distortion, assuming that the pupil of the system is at an image of the point light source as shown in Figure 12.8(a). A rotating

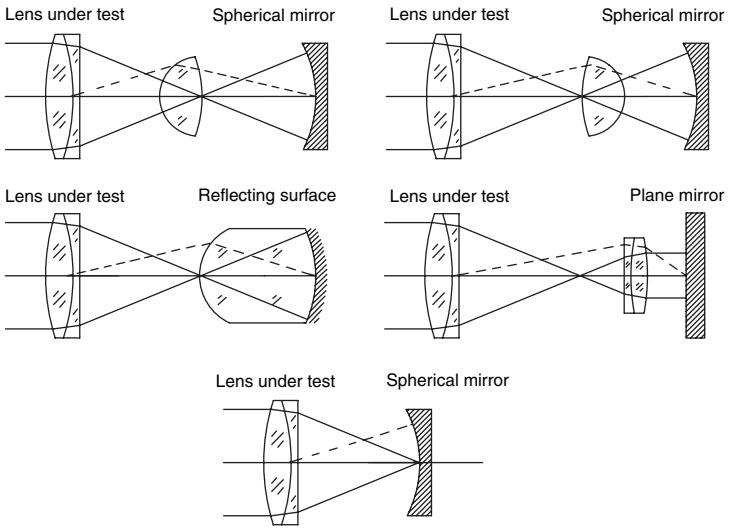

FIGURE 12.6. Systems to image the pupil of the optical element under test back on itself after reflection at the mirror.

ground glass in the plane of the interferogram might be sometimes useful in order to reduce the noise due to speckle and dust in the optical components. Ideally, this rotating glass should not be completely ground in order to reduce the loss of brightness and to keep the stop of the imaging lens at the original position, as shown in Figure 12.8(b). If the rotating glass is completely ground, the stop of the imaging

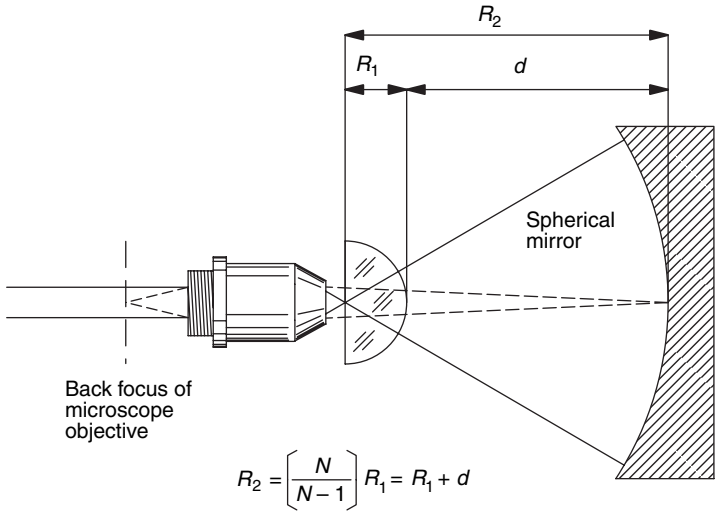

FIGURE 12.7. Dyson system to image the back focus of the microscope objective back on itself, after reflection on a concave mirror.

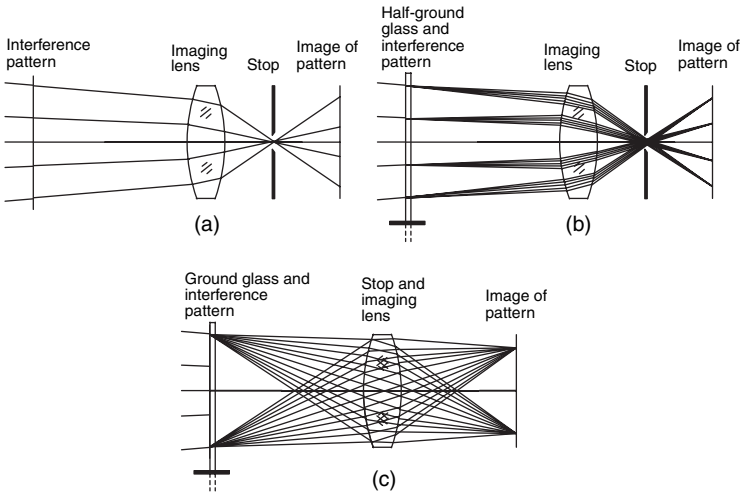

FIGURE 12.8. Imaging of the interferogram on the observation plane by means of a lens (a) without any rotating ground glass, (b) with a rotating half-ground glass, and (c) with a rotating fully-ground glass.

lens should be shifted to the lens in order to use all available light, but then the lens must be designed taking this new stop position into consideration as shown in Figure 12.8(c).

12.4. SOME NULL TESTING CONFIGURATIONS

Now some of the many possible configurations that allow a null test of an aspheric surface are reviewed.

12.4.1. Flat and Concave Spherical Surfaces

Not only aspheric surfaces are sometimes difficult to test, even spherical surfaces are difficult if the radius of curvature is too short or too large with respect to its diameter. Some null test configurations appropriate for flat or concave spherical surfaces are shown in Figure 12.9, with the relevant parameters and dimensions (Ritchey, 1904).

12.4.2. Telescope Refracting Objectives

A telescope doublet may easily be tested by autocollimation against an optical flat as shown in Figure 12.10. The flat must, of course, be as good as the rest of the system is intended to be. It is also necessary to keep the light source and the testing point as close as possible to each other to avoid astigmatism. When a system is double passed (including the case of the testing of a single concave surface at the center of curvature), as in this configuration, any antisymmetric wavefront aberration, like

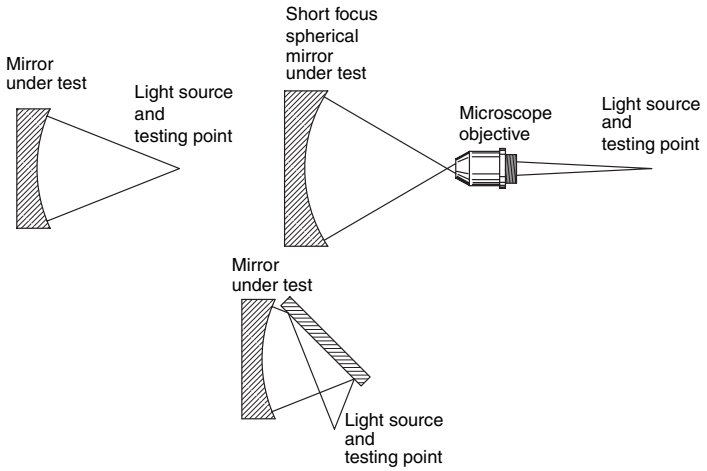

FIGURE 12.9. Testing concave spherical and flat mirrors.

coma, transverse color, and distortion, is canceled due to the the symmetry of the system.

12.4.3. Concave Paraboloidal Surfaces

If the paraboloid is not too large popular configurations use autocollimation with an optical flat as shown in Figure 12.11. The amount of spherical convexity or concavity permissible in the flat mirror used in autocollimation tests was shown by Burch (1938) to be given by

$$\delta = 64\left(\frac{f}{D}\right)^2 \frac{\varepsilon}{4Q - 0.5} \tag{12.4}$$

where F is the effective focal length and D is the aperture diameter of the system under test. The symbol δ represents the depth in fringes of the spherical concavity or convexity of the ''flat'' mirror, and ε represents the tolerance, also in fringes, of the

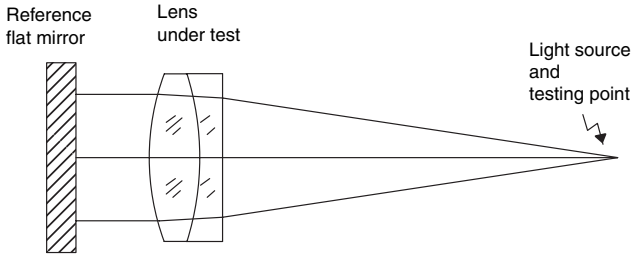

FIGURE 12.10. Testing a lens by autocollimation against a flat mirror.

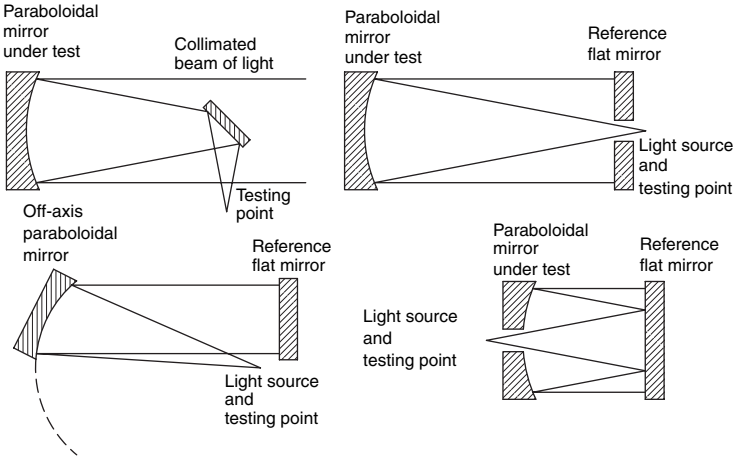

FIGURE 12.11. Testing paraboloidal concave mirrors.

zonal effect error introduced. If the system under test is refracting, the zonal error is $-2\varepsilon/(N-1)$, where N is the refractive index. The parameter Q is defined by

$$Q = -\frac{\text{OSC}}{\sin^2\theta} = \frac{1}{\sin^2\theta}\left(\frac{Y}{F\sin\theta} - 1\right) \tag{12.5}$$

where OSC is the ''offense against the sine condition'' and θ is the angle at which a marginal ray with height Yat the entrance pupil converges to the focus of the system. As Burch pointed out, a paraboloid and an aplanatic system are the two cases of practical interest: for these, $Q = 0.25$ and $Q = 0$, respectively, giving

$$\delta = \pm 128\left(\frac{F}{D}\right)^2 \varepsilon \tag{12.6}$$

If the paraboloid has a large aperture with respect to its radius of curvature, a point light source may be placed at its focus. Then, the collimated beam may be examined with another paraboloid with the same diameter but much larger focal length, as proposed by Parks (1974).

12.4.4. Concave Ellipsoidal or Spheroidal Surfaces

An ellipsoidal sometimes also called a prolate spheroid surface, obtained by rotation of the ellipse about it's major axis may be tested with conjugates at finite but at different distances (Kirkham, 1953) as shown in Figure 12.12(a). In a Twyman–Green interferometer, a configuration, like the one illustrated in Figure 12.13 and as suggested by Schwider (1999), can be used. Two identical lenses have to be used in both the arms of the interferometer, so that the aberration introduced by the lenses is the same.

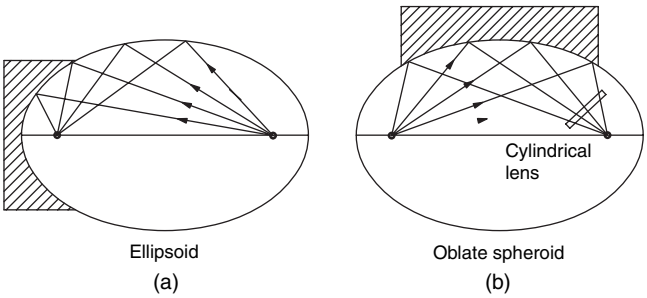

FIGURE 12.12. Testing concave ellipsoidal and oblate spheroidal mirrors.

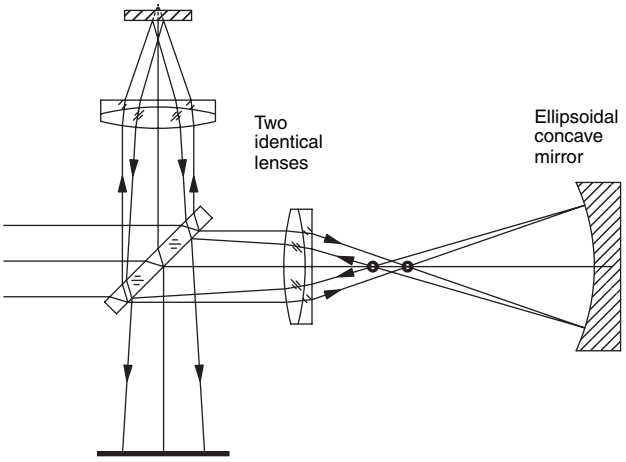

FIGURE 12.13. Testing and ellipsoidal concave mirror in a Twyman–Green interferometer.

An oblate spheroid is obtained by rotating the ellipse about its minor axis. In this case the images at the foci of the ellipse are astigmatic. Coma aberration is not present due to the symmetry of the system. A small cylindrical lens may be placed near its focus in order to correct this astigmatism if necessary (Everhart, 1966) as shown in Figure 12.12(b). Several different arrangements to test oblate spheroids using refractive compensators have been proposed, as described by Rodgers and Parks (1984).

12.5. TESTING OF CONVEX HYPERBOLOIDAL SURFACES

12.5.1. Hindle Type Tests

The testing of convex hyperboloids is very important for astronomical instruments. The most common test for these surfaces has been implemented by using a Hindle sphere as described in the following section. The problem with this method is that a

very large concave spherical surface, much larger than the surface under test, is required. Various other methods using compensators have been reported for testing convex hyperboloids, as described by Parks and Shao (1988).

We have mentioned that when testing conicoids a null test is obtained, then the center of curvature of the illuminating wavefront is at the proper focus; but since at least one of the geometrical foci is inaccessible, additional optical elements are required. A convex hyperboloidal surface can be tested with the method proposed by Hindle (1931), who showed how an autostigmatic arrangement for testing a convex hyperboloid can be implemented by retro-reflection from a sphere whose center is at the inaccessible focus of the hyperboloid as shown in Figure 12.14(a). Concave ellipsoidal surfaces can be examined with a Hindle arrangement, as shown in Figure 12.14(b). Small concave hyperboloids are also tested in a similar way (Silvertooth, 1940) as shown in Figure 12.14(c) A complete two mirror Cassegrain or Ritchey–Chrétien telescope can be tested in an autocollimating configuration devised by Ritchey if a large reference flat is available (see Fig. 12.14(d)).

Figure 12.15 shows Hindle arrangements for testing convex paraboloids and convex prolate spheroids. In addition to the Hindle sphere, a collimator is required to test a convex paraboloid. To test an ellipsoid (prolate spheroid), a lens designed for conjugates at finite distances is needed to provide a beam that converges to one of the spheroidal foci.

Although the Hindle and related tests for convex conicoids affords a stigmatic retroreflected image, its implementation is often impractical because keeping the obscuration inherent in the test within permissible bounds results in a prohibitively large spherical mirror. In the case of a hyperboloid of diameter D, the aperture of the Hindle sphere D_H is given by the relation

$$D_H = \frac{D(m+1)}{mr+1} \tag{12.7}$$

where r is the permissible obscuration ratio, and m is the magnification of the hyperboloid for its stigmatic conjugates. Thus, a 0.25-m hyperboloid with $m = 10$ and permissible $r = 0.2$ requires a 0.92-m Hindle sphere.

A modification of the Hindle test that avoids this difficulty was described by Simpson et al. (1974). Their arrangement is shown in Figure 12.16. The concave surface of a meniscus element serves as the Hindle sphere. This surface is half silvered so that it can be placed close to the conicoid without introducing obscuration. The radius of the convex surface can be chosen to compensate for the spherical aberration introduced by the refraction of the light beam passing through the concave surface. This testing configuration has been studied by Robbert (1979) and by Howard et al. (1983).

To test the effect of the meniscus Hindle element on the retroreflected wave, the hyperboloid is removed and the retroreflected image of S from a calibrating sphere with center at F is examined. Any significant aberration introduced by the meniscus can then be subtracted from the measurement of the figure error of the hyperboloid.

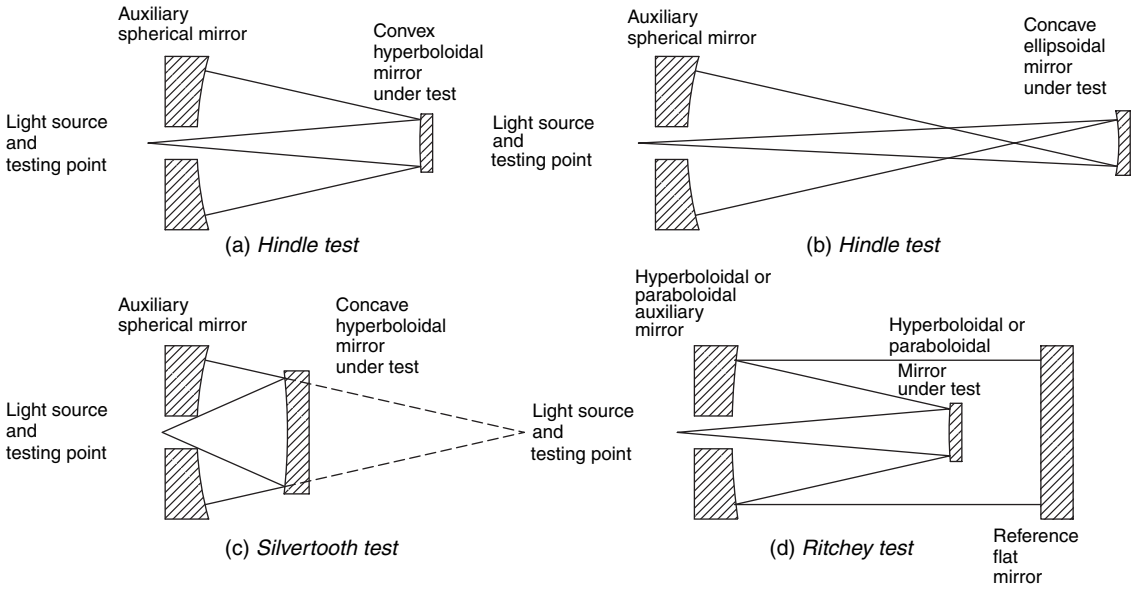

FIGURE 12.14. Hindle, Silvertooth, and Ritchey tests for hyperboloidal mirrors.

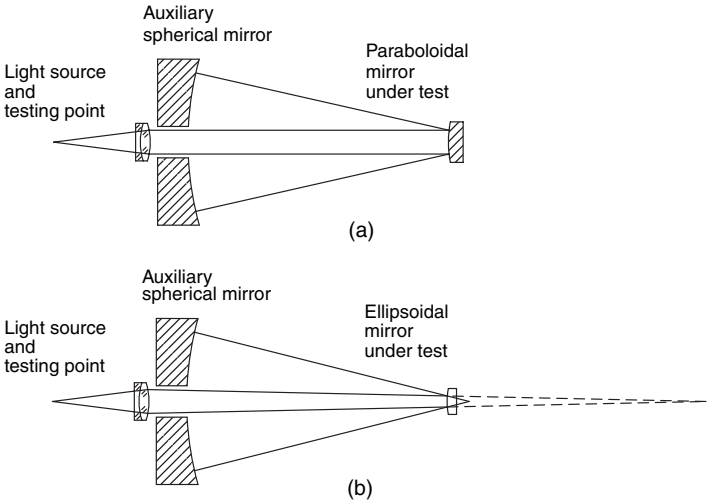

FIGURE 12.15. Testing paraboloidal and ellipsoidal convex mirrors.

A meniscus was designed to test the 0.25-m 10× hyperboloid mentioned earlier. The geometrical foci of the hyperboloid were at 0.6 and 6 m. The base radius of the hyperboloid is thus 1.33333 m, and its conic constant is $K = -1.49383$. Glass of index 1.52 was chosen for the meniscus element. For a 5 cm separation of the meniscus from the hyperboloid, the radius of the concave surface is 65 cm. With a meniscus thickness of 5 cm, the radius of the convex surface that results in aberration compensation at the edge of the aperture is 66.6637 cm. The required clear aperture of the meniscus is 0.254 m. The RMS (root mean square) of the wavefront deformations as given by the OPD (optical path difference) of the retroreflected wave is 0.0016 λ at $\lambda = 632.8$ nm. The stigmatic quality of the retroreflected image is thus retained in this modified Hindle test. Its use for testing convex conicoids is limited

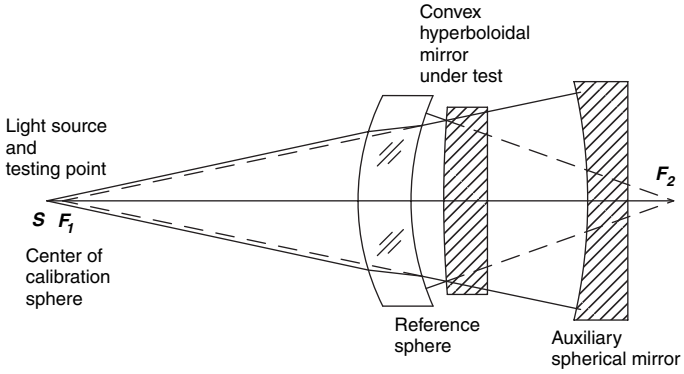

FIGURE 12.16. Simpson–Oland–Meckel modified Hindle arrangement.

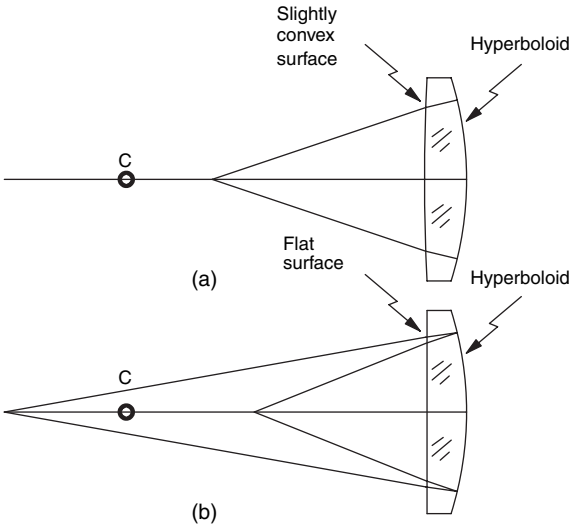

FIGURE 12.17. Meinel's test for a hyperboloidal convex mirror (a) using equal conjugates, with the light source and the testing point at the same position and (b) using unequal conjugates. The light source and the testing point are at different positions, but they can be made to coincide if a double-pass configuration is used, by placing a small flat mirror on these points.

only by the availability of refracting material of approximately the same size as the surface being tested.

An inconvenience with the Hindle test is that a large spherical mirror is needed. Another solution has been proposed by Meinel and Meinel (l983a, 1983b) in order to test the hyperboloid from the back surface. The mirror has to be made out of fused quartz in order to have good transparency and homogeneity. There are two possible optical arrangements for this test, one is shown in Figure 12.17(a) with the light source and the testing point at the same position. The surface has to be slightly convex with a long radius of curvature. As pointed out by Meinel and Meinel, a better solution is obtained if the back surface is made flat and the spherical aberration is completely corrected by locating the light source and the testing point along the optical axis, separated some distance from each other as shown in Figure 12.17(b). Many interesting variations of this test and some others may be found in a paper by Parks and Shao (1988).

12.5.2. Testing by Refraction

Descartes discovered that a refractive conical can focus an incident collimated beam of light without any spherical aberration, if the conic constant K is equal to

$$K = -\left(\frac{n_1}{n_2}\right)^2 \tag{12.8}$$

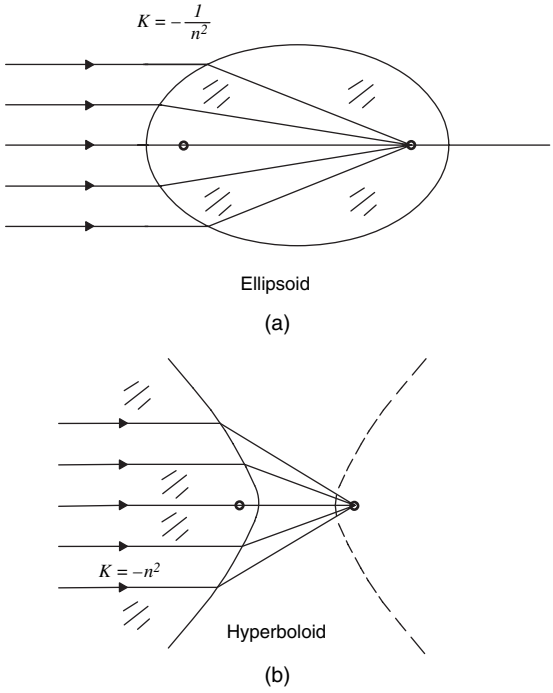

FIGURE 12.18. Cartesian configuration for an ellipsoid and a hyperboloid.

where n_1 is the refractive index of the first medium and n_2 is the refractive index of the second medium. There are two possible solutions:

(a) If $n_2 > n_1$ and $r > 0$, the conic is an ellipsoid, sometimes called Descartes ovoid, as shown in Figure 12.18(a). If the first medium is air and the second one is glass, we have a conic constant given by

$$K = -\frac{1}{n^2} \tag{12.9}$$

and if the distance from the vertex of the ellipsoid to the second focus, which is the point of convergence, is L, we have

$$Lc = \frac{n}{n-1} \tag{12.10}$$

where c is the vertex curvature.

(b) If $n_2 < n_1$ and $r < 0$, this is a hyperboloid, as illustrated in Figure 12.18(b). If the first medium is glass and the second one is air, the conic constant is

$$K = -n^2 \tag{12.11}$$

TABLE 12.1. Main parameter for the focusing of a collimated beam using a refractive conicoid with two common optical glasses.

	Refractive index	Ellipsoid		Hyperboloid	
	n	K	Lc	K	Lc
BK7	1.5168	−0.4347	2.9350	−2.3007	−1.9350
F2	1.6200	−0.3810	2.6129	−2.6244	−1.6129

and if the distance from the vertex of the hyperboloid to the focus, which is the point of convergence, is L, we have

$$Lc = -\frac{1}{n-1} \tag{12.12}$$

where the vertex curvature is negative.

Table 12.1 gives the main parameters for two common optical glasses.

Using this property, a convex hyperboloid may be tested with the arrangement given in Figure 12.19, if the index of refraction of the glass is of the proper value. The glass has to be clear and homogeneous; so optical glass or fused silica have to be used. Pyrex or glassceramic materials are not adequate. Since this test is made by transmission instead of reflection, the wavefront deformations OPD and the surface deformations W are related by $W = \mathrm{OPD}/2(n-1)$, which is about half the sensitivity obtained in a reflective arrangement.

If the refractive index is not adequate to produce an aplanatic image, an object distance may be selected so that the image is free of primary spherical aberration. This may be done by ray tracing, but an approximate solution may be calculated which requires that the third-order spherical aberration in Eq. (16.26) be zero. By making $n_{-1} = 1$ and defining a distance $l = y/u_{-1}$, this condition is

$$(8A_1 + Kc^3) + \frac{\frac{(n+1)}{l} + c}{n^2}\left(c + \frac{1}{l}\right)^2 = 0 \tag{12.13}$$

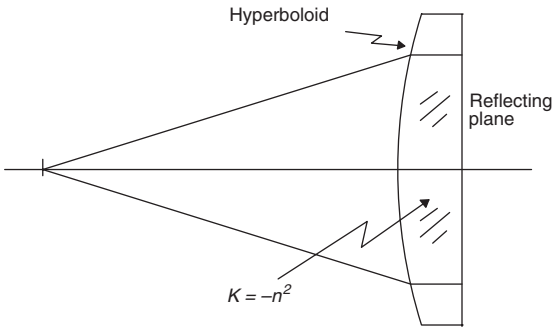

FIGURE 12.19. Testing a hyperboloid with a Cartesian configuration.

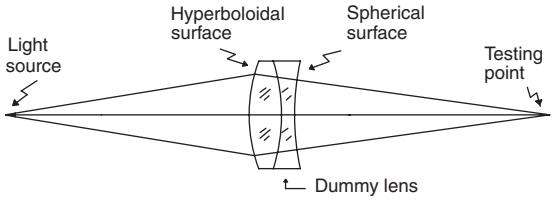

FIGURE 12.20. Testing an aspheric surface by selecting the conjugate distance that produces the minimum amount of spherical aberration.

Then, as suggested by James and Waterworth (1965), a lens with a convex hyperboloidal surface may be tested as shown in Figure 12.20. The spherical aberration of the second surface is eliminated by bringing this surface in contact with another lens using oil, whose second surface is spherical and is concentric with the testing point. In this case, however, the compensation is not perfect, since some small residual aberrations may remain. The sensitivity in about one fourth of that obtained in a reflective arrangement.

This property of the lenses with one hyperbolic convex surface can be used to test a convex surface with another procedure suggested by Bruns (1983). A convergent lens is placed in front of the convex surface under test to compensate for the spherical aberration introduced by the convex hyperbolic surface under test as illustrated in Figure 12.21. Unfortunately, no lens with spherical surfaces may correct the spherical aberration of the hyperboloid. So, Bruns uses a lens with a hyperboloidal surface. This hyperboloid in the front lens has conic constant K_L related to the selected glass refraction index. This makes the lens very simple to test when a collimated beam enters the lens through the flat face, since for this lens orientation spherical aberration is corrected. When this lens is used in reverse, that is, with the collimated beam entering the convex surface, it has a spherical aberration with the proper sign to cancel that of the convex mirror.

If the desired conic constant for the convex mirror is K_M, with radius of curvature R_M , Bruns has shown that the spherical aberration of this system is

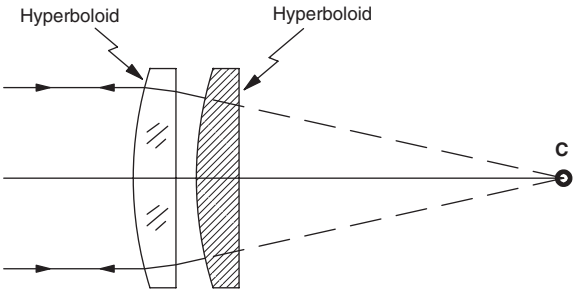

FIGURE 12.21. Testing a hyperboloidal surface by using an aspherical lens to compensate the spherical aberration.

compensated for when the refractive index n_L of the lens in front is given by the following relation:

$$K_M = -\frac{2(n_L + 1)(R_M + d)}{n_L(n_L - 1)R_M} \tag{12.14}$$

where d is the separation between the flat surface of the lens and the mirror, and an infinitely thin lens is assumed. The focal length of the lens is equal to $R_M + d$. The value of R_M is fixed, thus n_L and d must be chosen so that this relation is satisfied for the desired value of K_M.

12.6. TESTING OF CYLINDRICAL SURFACES

A concave cylindrical surface can be tested as illustrated in Figure 12.22, where the axis of the cylindrical test is in the vertical direction (Shnurr and Mann, 1981). A flat reference surface that reflects partially is located at the focus of the cylinder where the image is formed like a bright and narrow vertical line. The retroreflected wavefront is flat. It has to be noticed, however, that the wavefront is reversed about a vertical axis. Since the light is reflected twice on the surface under test, the antisymmetric mirror deformations are cancelled out while the symmetrical components are duplicated. Also, a highly spatially coherent illumination like that produced by a gas laser is needed.

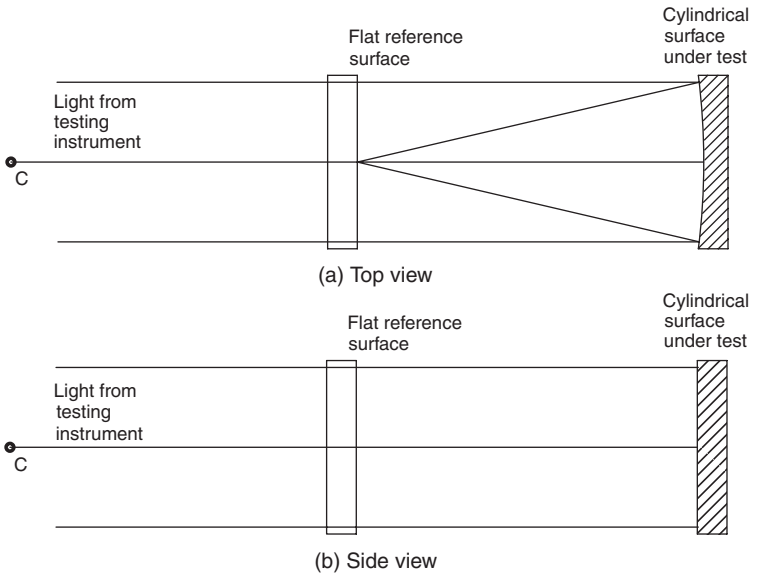

FIGURE 12.22. Testing a concave cylindrical surface in Twyman–Green interferometer using an auxiliary flat surface.

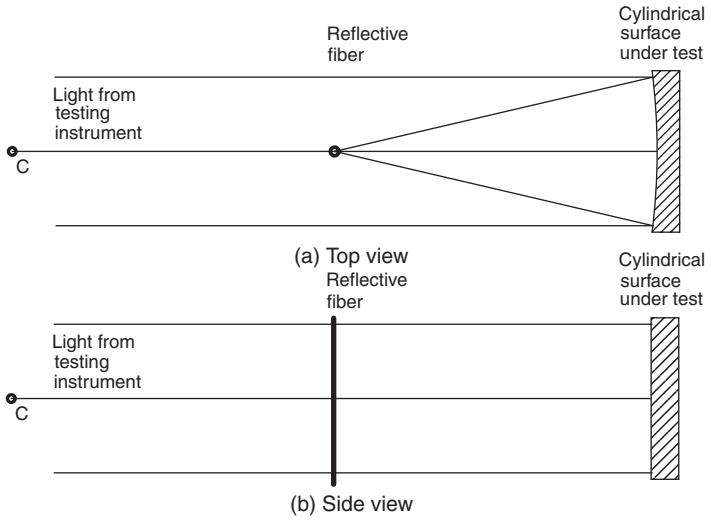

FIGURE 12.23. Testing a concave cylindrical surface in Twyman–Green interferometer using a reflective fiber.

Since the light being reflected is quite narrow, resembling a bright line, the reference mirror can be substituted by a very narrow mirror covering just the image and not the whole aperture. It must be remembered that this narrow image is not a perfect line due to the aberrations of the mirror under test. Geary and Parker (1987) and Geary (1991) substituted the narrow mirror by a thin fiber as shown in Figure 12.23. The fiber is coated to make it highly reflective and thinner than the width of the image due to the aberrations. The wavefront reflected back to the cylindrical surface on the fiber is cylindrical. Then, the aberrations are not duplicated due to the double pass, and the antisymmetrical components of the aberration are eliminated.

A cylindrical lens can also be tested using similar arrangements with a flat mirror as shown in Figure 12.24, or with a wire. The same conclusions as described in the last paragraph apply to this test.

A convex cylindrical mirror can be tested with the arrangement in Figure 12.25. The difference is that the beam from the interferometer has to be convergent. The retro-reflected wavefront is also spherical.

Another approach to test cylindrical lenses has been proposed by Lamprecht et al. (2003). The cylindrical wavefront produced by the cylindrical lens is transformed back to a plane wavefront by means of a diffractive optical element, which is made by optical e-beam lithography.

Q1

12.7. EARLY COMPENSATORS

This section on null compensators is adapted from the original chapter in earlier versions of this book, written by late Abbe Offner. The corresponding test of a

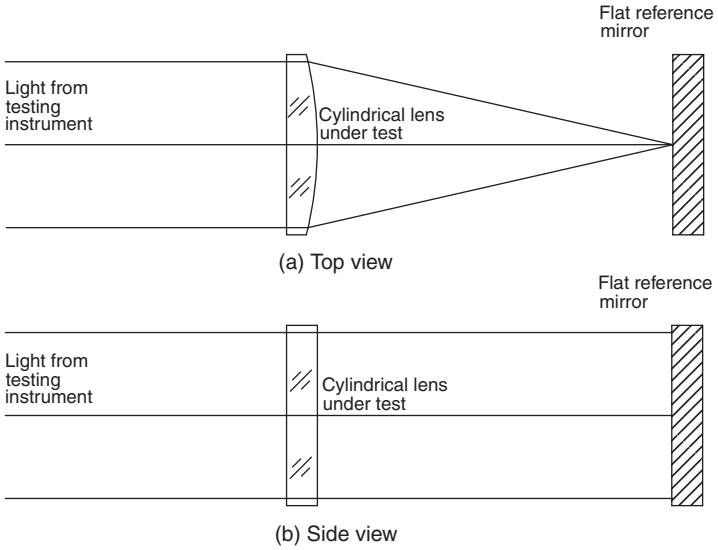

FIGURE 12.24. Testing a convergent cylindrical lens in Twyman–Green interferometer.

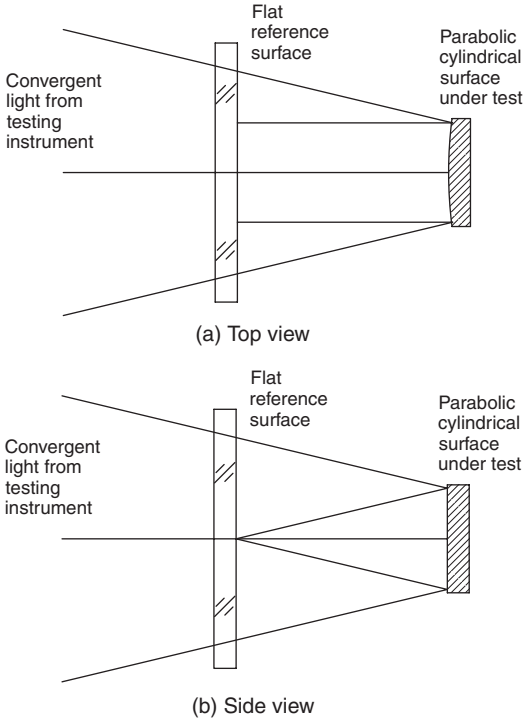

FIGURE 12.25. Testing a convex paraboloidal cylindrical surface with an auxiliary flat surface.

concave paraboloidal mirror is a lengthy and less accurate process. In this case, the figure errors must be deduced from measurements of the ray transverse aberrations (surface slopes) for a large number of zones, since a concave aspheric or conic surface tested at the center of curvature has a spherical aberration wavefront deformation given in third-order approximation by

$$W(\rho) = \frac{(8A_1 + Kc^3)\rho^4}{4} \tag{12.15}$$

where A_1 is the first aspheric deformation term, K is the conic constant, and $c = 1/R$ is the curvature. For a conic surface we may write

$$W = \frac{1}{4}KR\left(\frac{\rho}{R}\right)^4 \tag{12.16}$$ Q2

For many years the only alternative to the method of using the knife-edge test during the manufacture of a paraboloidal mirror was to test the mirror by autocollimation with the aid of an optical flat, which had to be as large and as accurately figured as the mirror being manufactured.

12.7.1. Couder, Burch, and Ross Compensators

Couder (1927) pointed out that departure from stigmatism of the image of a point source at the center of curvature of a paraboloidal mirror can be removed by interposing a small compensating lens between the image and the mirror. He used a two-element compensator in the arrangement shown in Figure 12.26. Two elements were necessary because he required a null corrector of zero total power to conveniently carry out the manufacturing process desired in his paper. To manufacture a 30-cm *f*/5 paraboloidal mirror, he used a null corrector whose aperture (scaled from his drawing) was about 4 cm.

The use of a spherical mirror beyond the center of curvature of a paraboloid to compensate for the aberrations of a paraboloid used with source and knife edge near its center of curvature was described by Burch (1936). He derived the fifth-order aberration of the null systems of this type and showed that with the two-mirror arrangement of Figure 12.27, the residual aberration of the paraboloid is less than one-fortieth of a wave for paraboloids as fast as $f/5$ and with apertures upto 80 cm,

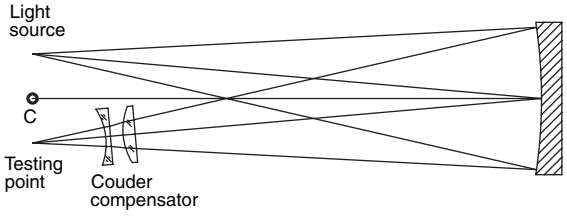

FIGURE 12.26. Couder two-element compensator.

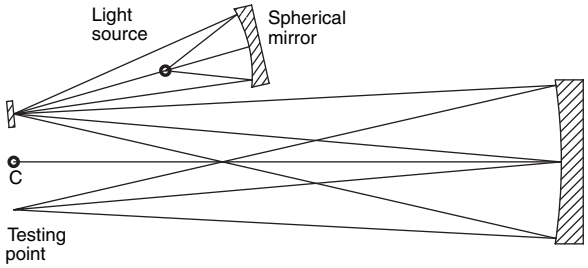

FIGURE 12.27. Burch two-mirror compensator.

when the compensating mirror aperture is one fourth of that of the paraboloid. For larger apertures and/or faster paraboloids, he suggested figuring the convex mirror with a down edge that departed from the base sphere by an eighth power law so that the seventh-order spherical aberration could be balanced. He calculated that an asphericity of about 2.8A would be required to compensate for the aberrations of the 5-m $f/3.33$ Mount Palomar mirror.

A simple third-order solution for a refracting compensator was also published by Burch (1938). The refractor was a planoconvex lens of focal length f and refractive index n, used in the arrangement shown in Figure 12.28, in which its plane surface is reflecting. For an paraboloid of base radius R, the third-order aberration of the image at the center of curvature is balanced when $f = Rn^2/(n-1)2$, so that for $n = 1.52$ the lens has an aperture of about one eighth of that of the paraboloid. Burch expected the residual aberration with this null corrector to be negligible for paraboloids of aperture ratio not exceeding $f/8$. He added, "Anyone with an aptitude for analytical optics or for ray-tracing could earn the gratitude of practical opticians by calculating the secondary aberrations for this and other kinds of compensating lens systems." This plea was answered 30 years later by Holleran (1968).

During the manufacture of the 5-m $f/3.33$ Mount Palomar mirror, a 25-cm diameter compensator was used to form a stigmatic retro-reflected image near the center of curvature of the mirror (Ross, 1943). The arrangement used is shown in Figure 12.29.

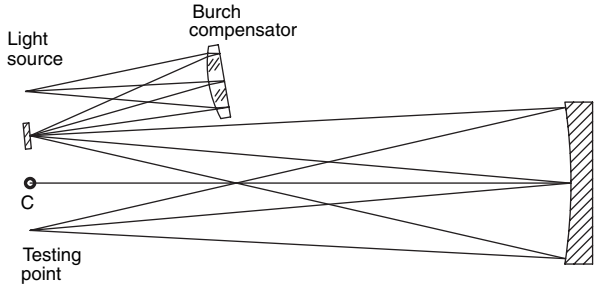

FIGURE 12.28. Burch planoconvex compensator.

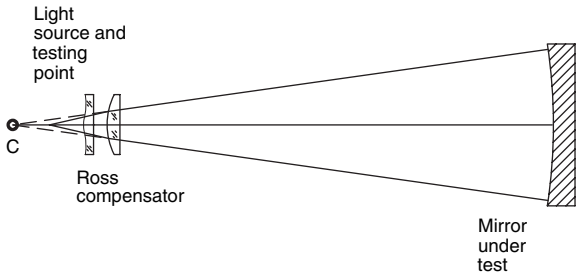

FIGURE 12.29. Ross aspheric compensator used during the fabrication of the 5-m Mount Palomar mirror.

To obtain a degree of compensation such that the residual zonal aberration resulted in a disk of confusion that was small compared to that caused by the atmosphere, Ross found it necessary to add an aspheric corrector plate to a refractive element with spherical surfaces, which by itself balanced the spherical aberration of the paraboloidal mirror. The retroreflective arrangement used by Ross has the advantage that it is coma-free and therefore insensitive to departures of the source and knife edge from the axis of the system. Moreover, since the compensator is used twice, it has to contribute only one-half as much aberration as is required in Couder's arrangement.

12.7.2. Dall Compensator

The planoconvex lens of Burch is a convenient and an easily used solution to the problem of making a null corrector for a paraboloidal mirror of moderate aperture. However, with this method a planoconvex lens used in the manufacture of a paraboloidal mirror can serve as a compensator only for other paraboloidal mirrors of the same focal length.

Dall (1947, 1953) noted that, since the spherical aberration of a lens is a function of its conjugates, the same planoconvex lens can be used as a compensator for many paraboloids. Dall employed the arrangement of Figure 12.30, which is quite similar to the arrangement used by Couder. The major difference is that, the Dall compensator is placed in front of the light source and not in front of the observer's eye. The reason for this is that if it is used on the convergent beam, the convergence of the

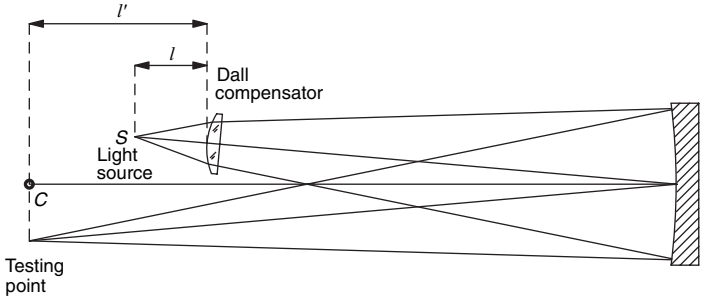

FIGURE 12.30. Dall planoconvex compensator.

beam may become so large that an observation of the whole surface under test may not be possible.

The Dall compensator is normally used in an off-axis arrangement, with the light passing only once through the compensator. Two double-pass configurations, with the divergent as well as the convergent beams passing through the compensator, may also be used: (a) exactly on axis, using a beam splitter and (b) slightly off axis. Then, the compensating lens needs to compensate only bale the total aberration on each pass, making it less strong. Then, an additional factor of 2 has to be used in front of Eq. (12.9). Another advantage of the double-pass symmetrical arrangement is that it is coma free. Thus, any coma introduced by the off-axis lateral displacement of the light source and the observer or any misalignment of the lens compensator does not introduce any coma. Unfortunately, the double-pass arrangement may be used only if the radius of curvature of the surface under test is very large compared with its diameter.

Dall found that proper choice of the short conjugate of the lens provides adequate compensation if the ratio of the radius of curvature R of the paraboloid to the focal length f of the lens is between 10 and 40. The relation required to balance the third-order aberration of the parabola at its center of curvature is

$$\frac{R}{f} = \frac{1}{2}(m-1)^2\left[\frac{n^2(m-1)^2}{(n-1)^2} + \frac{(3n+1)(m-1)}{n-1} + \frac{3n+2}{n}\right] \tag{12.17}$$

where m is the ratio of the long conjugate distance l' to the short conjugate distance l, and n is the index of refraction of the plano-convex lens. (The sign convention is such that in the Dall arrangement $m > 1$.)

The Dall compensator has been widely used, especially by amateur telescope makers. The degree of compensation that can be attained with this extremely simple null corrector is illustrated by the following example.

A Dall compensator is desired for a 0.6-m $f/5$ paraboloidal mirror. Taking $m = 2$, $N = 1.52$, and $F = 3$ m in Eq. (12.11), we find $R/f = 11.776$, which is within the bounds prescribed by Dall. The compensator specifications are then $f = 50.950$ cm, $l = -25.475$ cm, and $l' = -50.950$ cm. With this null corrector the computed root-mean-square (RMS) departure from the closest sphere [RMS optical path difference (OPD)] of the wavefront that converges to form an image of the light source is 0.048λ at $\lambda = 632.8$ nm. A paraboloid fabricated to give a null test with this compensator would have an RMS figure error of 0.024A. The Strehl intensity resulting from this figure error is 0.91. The diameter of the plano-convex lens required to achieve this compensation is about one-twelfth of that of the paraboloidal mirror.

The paraboloid of the examples is about the largest for which a Dall compensator is adequate. Since the arrangement suggested by Dall is not coma-free, the light source must be located accurately on the axis of the convex lens, and this axis should be directed to pass through the pole of the paraboloid.

Practical instructions for making and using a Dall null tester are given in two papers by Schlauch (1959) and by Stoltzmann and Hatch (1976). By restricting the

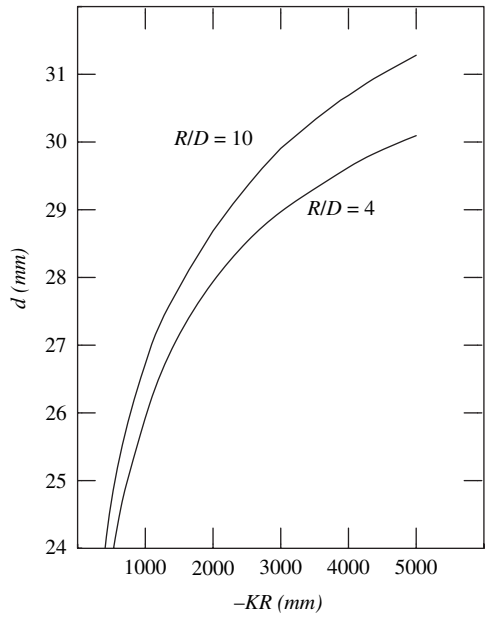

FIGURE 12.31. Distance d from the light source to the Dall compensator lens in Figure 12.32 for different values of the product of the radius of curvature times the conic constant.

refractive index of the plano-convex lens to 1.52, the computation of Eq. (12.11) can be avoided with the help of a curve in Schlauch's paper, which is adapted from the one published by Dall (1953).

A Dall lens made with BK-7 glass and using red light can also be calculated with the curves in Figure 12.31. The radius of curvature is 25 mm and the thickness is 5 mm. A difference with Figure 12.30 is that it has been assumed that the plane surface of the lens and the testing point (knife edge) are in the same plane, as illustrated in Figure 12.32. Assuming only the presence of third-order spherical aberration, from Eq. (12.10) we may say that the distance d from the light source to the vertex of the convex surface of the lens has to be a function only of the product KR. This is true only for small apertures (large ratio R/D). If the aperture is large (ratio R/D small), the fifth-order spherical aberration is present in the Dan lens, and it

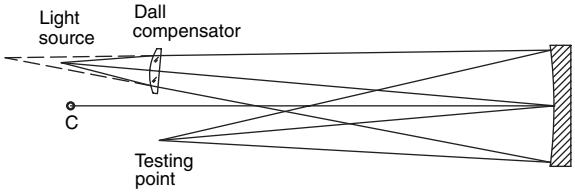

FIGURE 12.32. A Dall compensator. The testing point is assumed to be at the same plane as the flat surface of the Dall lens.

has to be partially compensated with some overcompensation of the third-order aberration. Then, a zonal spherical aberration remains uncorrected. This remaining aberration is not a severe problem if the aperture is small or if there is a large central obscuration, as pointed out by Rodgers (1986).

A Dall compensator can be modified to be coma-free by using the planoconvex lens on axis like in the retro-reflective arrangement of Ross. The relation to be satisfied with this arrangement is a modification of Eq. (12.11) in which the factor 1/2 is eliminated since the lens is traversed twice. With this arrangement, for example, the compensator for the $0.6-mf/5$ paraboloid has $R/f = 23.552$, $f = 25.475$ cm, $l = -12.737$ cm, and $l' = -25.475$ cm. The diameter of the planoconvex lens is then that of the paraboloid. The residual figure error of the paraboloid that gives a null test with this arrangement is exactly the same as that computed in the preceding example. The retroreflective arrangement has the advantage, however, that since it is coma-free, it is not affected by small departures of the light source from the axis of the planoconvex lens.

In an interesting variation of the Dall compensator proposed by Puryayev (1973), an afocal meniscus whose concave surface is conicoidal is substituted for Dall's planoconvex lens in the autostigmatic arrangement used by Ross (Fig. 12.29). For an afocal meniscus,

$$r_1 - r_2 = \frac{d(n-1)}{n} \tag{12.18}$$

where r_1 is the radius of the concave surface of the meniscus, r_2 is the radius of its convex surface, d is its thickness, and n is its index of refraction.

The third-order value of the conic constant K of the concave surface required to compensate for the aberration of a paraboloid of radius R is

$$K = \frac{R}{(N-1)\left(\dfrac{r_2}{r_1}\right)^2 l} \tag{12.19}$$

where l is the distance from the light source to the meniscus. (The sign convention is such that K is negative.)

With the same 20-cm-diameter meniscus compensator, Puryayev achieved compensation for any paraboloidal or near-paraboloidal surface whose focal length does not exceed 24 m and whose aperture ratio does not exceed 1:4. The maximum residual wave aberration of the retro-reflected wave for any paraboloid in this range is about $\lambda/2$ at 632.8 nm. This residual can be computed and taken into account when the figure of the test mirror is being determined.

12.8. REFRACTIVE COMPENSATORS

As described earlier (Burch, 1936; Ross, 1943), compensation for the spherical aberration of a paraboloid or other aspheric concave mirror can be achieved to any

desired degree of accuracy by the incorporation of an aspheric element in the null corrector. This method is limited to cases in which the figure of the aspheric element can be ascertained with an accuracy better than that desired for the aspheric mirror. Primary mirrors that are to be incorporated into diffraction-limited space-borne optical systems are now required to have RMS figure errors as small as one-hundredth of the wavelength of visible light. It is therefore desirable that the components of a null corrector for these mirrors be spherical or flat so that their figure errors can be measured to the required accuracy.

In the design of his null corrector, Ross found that the farther he put the lens from the center of curvature of the mirror, the less residual aberration there was when the compensation was exactly at the center and the edge. This is so because, although the longitudinal spherical aberration S of the normals to the paraboloid follows the simple law $S = y^2/2R$, where y is the distance of the normal from the axis of the paraboloid and R is its radius, additional terms of a power series would be required to describe the same spherical aberration distribution in a coordinate system with its origin at the null corrector. For a null corrector in contact with the paraboloid, the compensating spherical aberration would be described by the same simple law. Unfortunately, this null corrector would be as large as the paraboloid.

12.8.1. Refractive Offner Compensator

Offner (1963) pointed out that a small lens that forms a real image of a point source at the center of curvature of a paraboloid, in combination with a field lens at the center of curvature that images the small lens at the paraboloid, is optically equivalent to a large lens at the paraboloid. The use of a field lens in this way was first suggested by Schupmann to control secondary spectrum (Schupmann, 1899; Offner, 1969). This kind of compensator has been widely used to test astronomical optics of many different characteristics (Sasian, 1988).

With a field lens that images the compensating lens c at the paraboloid in Offner's arrangement, the spherical aberration of the compensating lens must follow the same law for aperture as do the normals to the paraboloid.

This restriction on the compensating lens is not necessary. All that is required is that lens c provide sufficient third-order spherical aberration to compensate for that of the normals of the paraboloid. The power of the field lens (and thus the location of the image of lens c) is then varied to minimize the high-order aberration.

To balance the third-order aberration of the normals to a conicoidal mirror with conic constant K and base radius R, a planoconvex lens of focal length f and index of refraction N must satisfy the relation

$$-\frac{KR}{f} = (1-m)^2\left[\frac{n^2(1-m)^2}{(n-1)^2} + \frac{(3n+1)(1-m)m}{n-1} + \frac{(3n+2)m^2}{n}\right] \qquad (12.20)$$

where m is the ratio l'/l (Fig. 12.33). (The conicoid must have $K < 0$ if the aberration of its normals are to be balanced by the spherical aberration of a planoconvex lens. The sign convention is such that $m < 0$.)

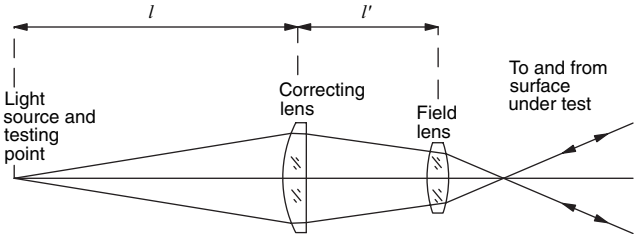

FIGURE 12.33. Refracting compensator with field lens.

Since the mirror under test in general has a large spherical aberration, the field lens does not have an ideal position. It may be placed between the mirror and its caustic, inside the caustic region or outside the caustic. Any of these possible locations produce good compensations, with slight variations, as explained by Sasian (1989). Different techniques for designing this compensator have been explored by several authors, among others, by Landgrave and Moya (1987) and by Moya and Landgrave (1987).

The main purpose of the field lens is to avoid fifth-order spherical aberration, but another equally important consequence of its presence is that the wavefront at the mirror under test is imaged on the plane where the aberrations are observed, that is, at the compensating lens.

The importance of the field lens in the Offner arrangement is evident from the example of the design of a null corrector for a 1-m $f/4$ paraboloid using planoconvex lenses with refractive index 1.52. The quantity m that results in the desired convergence angle of the retroreflected wavefront is first chosen.

Choosing a convergence of $f/12$ leads to $m = -0.6667$. The value of the focal length of the compensating lens required to balance the third-order aberration of the paraboloid normals is then seen from Eq. (12.14) to be 20.9115 cm, since $K = -1$ and $R = 800.0$ cm. The conjugates for $m = -0.6667$ are $l = -52.2772$ cm and $l' = -34.8532$ cm. The retroreflective system formed by placing the source at the long conjugate of this lens and the paraboloidal mirror center of curvature at its short conjugate is corrected for third-order spherical aberration, but has fifth-order lateral spherical aberration of -0.0205 mm. The RMS OPD of the retroreflected wavefront is 0.23 λ at $\lambda = 632.8$ nm.

A field lens of focal length 33.3976 cm at the center of curvature of the paraboloid forms an image of the compensating lens on the paraboloidal mirror. With this addition, the sign of the fifth-order spherical aberration is reversed, its value being $+0.0207$ mm. The RMS OPD of the retroreflected wave is increased slightly to 0.26 λ.

The focal length of the field lens that minimizes the high-order spherical aberration is found to be 66.8900 cm. With this field lens, the computed RMS OPD of the retroreflected wavefront is reduced to 0.0003 λ, a value well below what can be measured. The diameter of the compensating lens required for this degree of correction is one-twentieth that of the $f/4$ paraboloid.

In Eq. (12.14), it is assumed that the curved surface of the planoconvex field lens is at the center of curvature of the paraboloid. It is sometimes convenient to move the field lens to a position close to, but not at the center of curvature. In this case the field lens introduces an additional magnification m_f The condition for compensation of third-order aberration then becomes

$$-\frac{KR}{f_f^2} = (1-\bar{m})^2\left[\frac{n^2(1-\bar{m})^2}{(n-1)^2} + \frac{(3n+1)(1-m)\bar{m}}{n-1} + \frac{(3n+2)\bar{m}^2}{n}\right] \qquad (12.21)$$

where $\bar{m} = {m_f}^2/m$.

Like Ross's arrangement, the retroreflective arrangement of Offner is inherently coma-free so that the correction of the retroreflected wavefront is maintained when the source is near the axis but not exactly on it.

The high degree of stigmatism that can be achieved by the use of the Offner corrector has led to its application for the quantitative assessment of the figures of large aperture concave conicoidal mirrors. For this purpose, the retroreflected wavefront can be compared with a reference sphere in a spherical wave interferometer (Houston et al., 1967). A multipass version of the spherical wave interferometer in which the retroreflected wavefront and the reference sphere are optically conjugate (Heintze et al., 1967) is particularly useful for making this measurement with the greatest accuracy. With this interferometer, which has been given the acronym SWIM (spherical wave interferometer multibeam), individual points of a wavefront have been measured with an accuracy of 0.003 λ (private communication).

12.8.2. Shafer Compensator

This compensator is a triplet, designed by Shafer (1979), so that the following three conditions are satisfied:

1. For a certain distance from the light source to the compensator, the spherical wavefront from the light source preserves its spherical shape after passing through the compensator. Then, positive or negative compensations may be achieved by displacing the system along the optical axis.
2. The system is afocal (effective focal length infinite), so that the angles with respect to the optical axis of the light rays entering the system are preserved after passing through the compensator.
3. The angular magnification of the afocal system, (lateral magnification for a near object) must be equal to $+1$. Thus the apparent position of the light source does not change when moving the compensator along the optical axis.

A system with a negative lens between two positive lenses, as in Figure 12.34, is appropriate for positive conic constants (oblate spheroids) of any magnitude and negative conic constants (paraboloids or hyperboloids) of moderate magnitude as

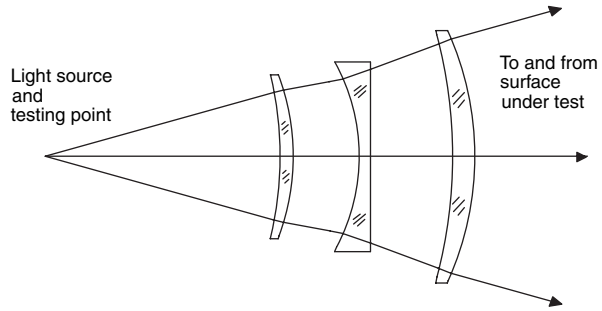

FIGURE 12.34. Shafer compensator with all lenses made with BK-7 glass.

shown in the graph in Figure 12.35. This graph is inverted when a positive lens is placed between two negative lenses.

12.8.3. General Comments about Refracting Compensators

The main refracting compensators are the Couder, Dall, Shafer, and the Offner compensators. They have the following properties in common:

1. All compensate the spherical aberration but with a different degree of perfection. The best in this respect is the Offner compensator.
2. All can be used in a single or double pass, but the Couder and Dall compensators are typically used in a single pass, generally in front of the light source, while the Shafer and Offner compensators are normally used in double pass.

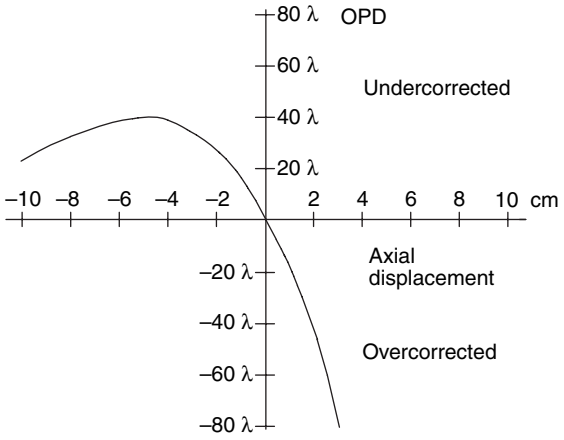

Q3 **FIGURE 12.35.** Wavefront aberration due to third-order spherical aberration vs. lens motion for Shafer compensator and an *f*/2 system with a wavelength of 632.6 nm.

3. The chromatic aberration is not corrected in any of these compensators, hence monochromatic light has to be used. One possibility is to use laser light and another is to use a color filter. It is suggested to use a red filter close to the eye or image detector (after the compensator) so that the wavefront shape is not affected by this filter.

4. The amount of spherical aberration correction depends very critically on the axial position of the compensating lens; so unless its position is very accurately measured, we can never be sure about the exact value of the conic constant of the concave surface under test. This value has to be measured by some other test that does not use any compensator, like the Hartmann test. However, the general smoothness of the surface can be easily determined only with a compensator.

5. In a double-pass configuration, any lateral displacement of the light source and the observer in opposite direction and by equal amounts, with respect to the optical axis, does not introduce any coma. It is assumed, however, that the optical axis of both the conic surface under test and the compensating lens coincide; otherwise some coma is introduced.

12.9. REFLECTING COMPENSATORS

The weak point in making measurements with the Offner null corrector is the difficulty in measuring the index variations of the nulling element to the required degree of accuracy. In the example described (Offner, 1963), the thickness of the 4.5-cm-diameter compensating lens was 1.05 cm. An average index difference of 3×10^{-7} along the paths of the two rays that traverse this lens twice results in an optical path difference of $\lambda/100$ at $\lambda = 632.8$ nm. Faster aspheric mirrors with Larger aperture require larger compensating lens diameters and thicknesses. For these, even smaller average index differences result in optical path errors of this magnitude. Fabrication and qualification of large glass elements to this degree of homogeneity is not feasible at present.

These difficulties can be avoided by substituting spherical mirrors for the planoconvex refracting compensating element of Figure 12.33. The figure errors of such elements can be determined with great accuracy. A small field lens can be retained since it is possible to select small pieces of glass with satisfactorily small index variations.

It is well known (Burch, 1936) that the axial aberration of a spherical mirror used at a magnification other than -1 can be used to compensate for the aberration of the normals of a concave conicoid with negative conic constant. The high degree of compensation achieved with the Offner refractive null corrector can also be obtained by a reflecting compensator used with a field lens at the center of curvature of the conicoid, as shown in Figure 12.36. As in the refractive version, the radius of the nulling mirror R_N and its conjugates l and l' are chosen to balance the third-order aberration of the normals to the conicoid of radius R_c and the conic constant K. The power of the field lens is then

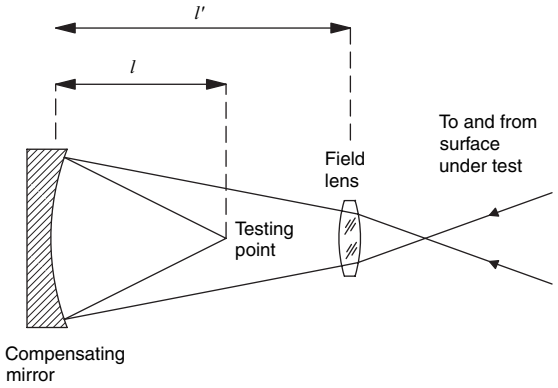

FIGURE 12.36. Single mirror compensator with field lens.

varied to minimize the high-order aberration. The relations to be satisfied are as follows:

$$R_N = -\frac{8KR_c}{(m^2-1)^2} \tag{12.22}$$

$$l = \frac{(1-m)R_c}{2} \tag{12.23}$$

$$m = \frac{l}{l'} = -\frac{2\eta_c}{\eta_N} \tag{12.24}$$

where $2\eta_c$ and $2\eta_N$ are the f numbers of the beam at the center of curvature of the conicoid and at the retroreflected image, respectively.

The ratio of the diameter of the conicoid D_c to that of the null mirror D_N can be computed from the relation

$$\frac{D_c}{D_N} = \frac{(m^2-1)^2}{4K(m-1)} \tag{12.25}$$

Some values of the ratio of the diameter of a paraboloid to that of a single mirror compensator, computed from Eq. (l2.19), are listed in Table 12.2. Diameter ratios of more than 10 require values of $-m$ greater than 4. A practical limit on the value of m is set by the resultant value of h_N, the f number at the retroreflected image, which is inversely proportional to m [Eq. (12.18)]. If the compensated wavefront is to be examined interferometrically without transfer optics, the interferometer must be capable of handling f/η_N beam. The single-mirror compensator thus requires large compensating mirrors if η_c, the f number of the conicoidal mirror, is small. The permissible residual aberration of the compensated image also must be taken into account, and in some cases this results in a value of A_c greater than that set by the lower limit on η_N.

TABLE 12.2. Diameter ratio and magnification, single mirror compensator.

Magnification	Diameter ratio
−3	4
−3.5	7
−4	11.25
−4.5	16.8
−5	24

For example, a one-mirror compensator was designed for a 3-m $f/2.45$ hyperboloidal primary mirror of a proposed Ritchey–Chrétien system. The conic constant of the mirror was −1.003313. A value of −4.9 was chosen for m, resulting in an $f/1$ beam at the retroreflected image. The third-order mirror specifications computed from Eqs. (12.4) to (12.7) and the specifications of the optimized design are shown in Table 12.3. The focal length of the field lens that minimizes the high-order aberration is 55.4849 cm. The computed RMS OPD of the retroreflected wavefront is 0.009 λ at $\lambda = 632.8$ nm. If a smaller residual had been required, a smaller value of $-m$ would have been chosen for the compensator. The resulting compensator mirror would then have been larger, and the convergence angle of the retroreflected beam would have been smaller.

12.9.1. Reflective Offner Compensator

Although the single-mirror compensator of Figure 12.36 is optically the least complicated of the reflecting compensators, practical implementations require an additional element, such as the folding flat of Figure 12.37, to make the retroreflected image accessible. The quality of the flat must, of course, be comparable to that of the spherical mirror.

The same number of accurately fabricated optical components is required in the two-mirror compensator shown in Figure 12.38. The in-line arrangement facilitates accurate alignment and provides an accessible retroreflected image.

With the two-mirror compensator, the central portion of the aspheric mirror cannot be observed because of the holes in the nulling mirrors. These null correctors should be designed so that the obscured portion of the aspheric mirror in the null test is no larger than the obscured portion of the aspheric mirror in actual use.

The third-order design of a two-mirror compensator is affected by the value of the obscuration ratio at each of the mirrors. The following equations apply when the

TABLE 12.3. One-mirror null corrector for 3-m $f/2.45$ hyperboloid:

Type of design	m	R_N	l	A_N	η_N
Third order	−4.9	22.2849	65.7404	13.42	1.000
Optimized	−4.7	22.2849	65.7518	13.5	1.044

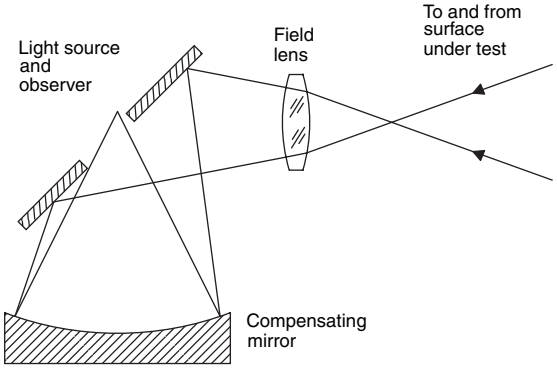

FIGURE 12.37. Practical implementation of single-mirror compensator.

obscuration ratio r is the same at the two mirrors. As in the case of the single-mirror null corrector, the parameters and apertures are functions of a magnification. For the two-mirror compensator, the magnification is that from the intermediate image to the image at the center of curvature of the aspheric mirror, defined by the relation

$$m_1 = -\frac{2\eta_c}{\eta_1} \tag{12.26}$$

where η_1 is the f number at the intermediate image. The ratios of the diameters of the apertures of the two nulling mirrors D_1 and D_2 to the aperture of the conicoid D_c when the third-order aberration of the conicoid normals is compensated for by that of the null corrector can be computed from the following relations:

$$\frac{D_c}{D_1} = \frac{1}{4K}(m_1 + 1)\left[m_1^2(1 + 2r - r^2) - 2m_1(1 - r) - 2\right] \tag{12.27}$$

$$\frac{D_c}{D_2} = \frac{D_c}{D_1}\frac{m_1 r - 1}{m_1 + 1} \tag{12.28}$$

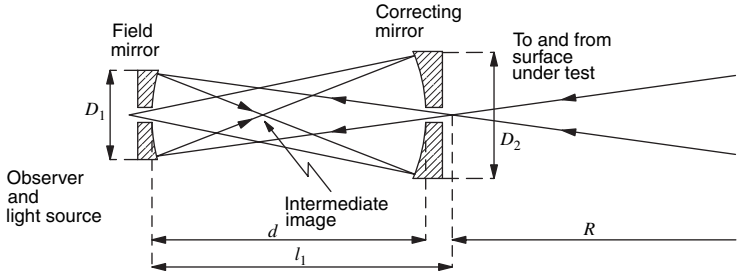

FIGURE 12.38. Two-mirror compensator with field lens.

The other relations required for the third-order design are as follows:

$$R_1 = \frac{4D_1\eta_c}{1 - m_1} \tag{12.29}$$

$$R_2 = \frac{4D_2\eta_c}{m_1(2 - r) + 1} \tag{12.30}$$

$$l_1 = 2\eta_c D_1 \tag{12.31}$$

$$d = \eta_1(D_1 + D_2) \tag{12.32}$$

$$\eta_N = -\frac{2\eta_c}{m_1(1 - r) + 1} \tag{12.33}$$

where l_1 is the distance from the center of curvature of the conicoid to the field mirror, d is the distance between the two mirrors, and η_N is the f number at the retroreflected image.

The way in which the apertures of the two mirrors and the f number of the retroreflected image vary as a function of the magnification m for two values of the obscuration ratio can be seen in Table 12.3. Comparison with Table 12.1 shows that for a given magnification, the larger mirror of the two-mirror compensator is approximately of the same size as the single-mirror compensator. However, the difference between the magnitudes of m_1 and $2\eta_c\eta_N$ in Table 12.3 indicates that, for a given maximum size compensator element, the convergence angle at the retroreflected image with the two-mirror compensator is approximately one half of that with a single-mirror compensator.

The degree of compensation attainable with the two-mirror compensator is extremely high as shown by the following example. A compensator was required for a 3-m $f/1.5$ paraboloid that was to be used with an obscuration ratio of 0.3. A spherical wave interferometer that could accommodate convergence angles up to $f/1.2$ was available. The values $r = 0.25$ and $m_1 = -4$ were chosen to give the safe value $\eta_N = 1.5$. Equations (14.9) and (14.10) led to the acceptable values $A_1 = 14.82$ cm and $A_2 = 27.22$ cm. The parameters obtained from Eqs. (12.15) to (12.19) are listed as third-order design parameters in Table 12.4. The field lens required to optimize this compensator is a meniscus lens of refractive index 1.519, thickness 0.5 cm, and radii 14.619 cm (convex) and 71.656 cm (concave), with the convex surface facing the paraboloid. With this field lens and the slight modifications of the other parameters shown in Table 12.4, the RMS OPD of the retroreflected wavefront is 0.009 λ at $\lambda = 632.8$ nm. Had a smaller residual aberration been

TABLE 12.4. Two-mirror null corrector for 3-m f/1.5 paraboloid.

Type of design	m_1	R_1	R_2	l_1	d	A_2	η_N
Third order	− 4.00	17.7778	22.2222	44.4444	27.7778	22.22	1.50
Optimized	− 3.99	17.7776	22.2227	44.3868	27.7789	21.34	1.52

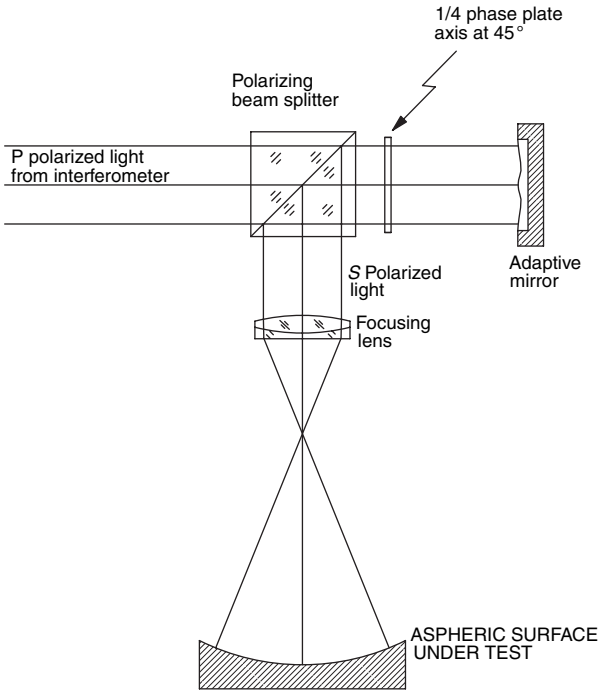

FIGURE 12.39. Aspheric compensator using an adaptive mirror.

required, the value *of* m_1 would have had to be reduced. This would have resulted in larger values of A_1 , A_2, and η_N.

12.9.2. Reflective Adaptive Compensator

Another interesting reflective compensator has been described by Tiziani et al. (2001). They use an optical configuration where the reflective compensator is an adaptive mirror whose shape can be changed as desired by controlling it with a computer. The system in Figure 12.39 adds the reflected wavefront from the aspheric surface under test to the shape of the adaptive mirror. The light beam is reflected twice on the adaptive mirror, so that its shape is added twice to the aspheric wavefront from the system under test. The flexible mirror is an aluminum coated nitride membrane that is attracted electrostatically by electrodes on the back of the membrane. This membrane can be deflected up to about 20 μm PV, which corresponds to about 80 wavelengths due to the double reflection on this membrane.

12.10. OTHER COMPENSATORS FOR CONCAVE CONICOIDS

The success of the simple small compensators described in the preceding sections results from a fortunate combination of conditions.

1. The concave aspheric mirrors by themselves transform the divergent wave from a point source to a convergent one though aberrated wave.
2. The greater part of the aberration introduced by the aspheric is of low order.
3. The sense of the aberration is opposite to that introduced by a concave mirror or a simple convex lens.

The first condition must be met if the null corrector is to be smaller than the aspheric mirror being tested. The second condition makes it possible to get good compensation with a single element of convenient form. The third condition makes it possible to use a simple relay lens that provides a position for a field lens. Concave spherical mirrors can be used for compensators only when this condition is met.

A small null corrector of the same general form can be designed for any concave mirror whose surface is generated by rotating a conic section about its major axis.

Concave prolate spheroids do not require compensators since their geometrical foci are accessible and, as is the case with all conicoids that have geometrical foci, their imagery is stigmatic when these are the conjugates. However, when one of the geometrical foci is at a large distance from the mirror, it may be more convenient to perform a null test at the center of curvature with one of the null correctors described in Sections 12.2–12.4.

An oblate spheroid, such as the one that is used as the primary mirror of a Wright–Schmidt system, does not satisfy condition 3. Nevertheless, a null test of the modified Dall type can be obtained by substituting a plano-concave lens for the Dall plano-convex lens (Figure 12.40). Since the curved surface of this lens faces the oblate spheroid, the third-order solution is formally the same as that for the Offner plano-convex compensator. The parameters and conjugates of the plano-convex lens required to balance the third-order aberration of the normals to the prolate spheroid can thus be obtained by the use of Eq. (12.14). The quantity m is the ratio l'/l. In this case it is positive and has a value less than 1. The effect of the choice of m on the ratio of the size of the oblate spheroid to that of the null corrector is shown in Table 12.5; the values were computed for $N = 1.52$ and $K = 1$. The implementation of the value

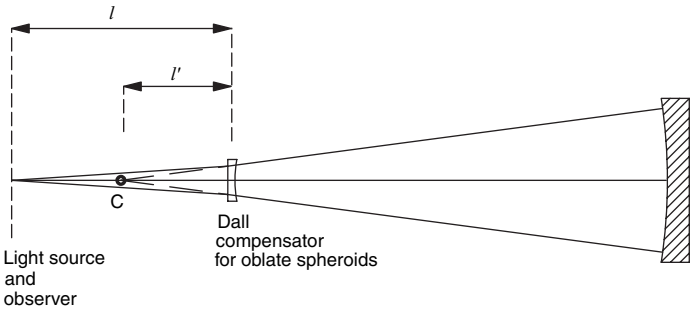

FIGURE 12.40. Modified Dall compensator for oblate spheroids.

TABLE 12.5. Aperture of planoconcave null lens compensator for oblate spheroid ($K = 1, n = 1.52$).

m	Diameter asphere/Diameter compensator
0.0	8.54
0.1	7.13
0.2	5.88
0.3	4.77
0.4	3.8

$m = 0$ requires the addition of a collimator to put the source optically at an infinite conjugate. The resulting arrangement is shown in Figure 12.41.

A null corrector of this type was designed for a 0.6-m aperture $f/5$ oblate spheroid with conic constant $K = 1$. The departure of this aspheric from the base sphere is equal in magnitude but opposite in sense to that of the paraboloid used as an example in Section 12.2. The values $n = 1.52$ and $m = 0$ were chosen. The focal length of the planoconcave lens, obtained from Eq. (12.10), is 70.2216 m. The RMS OPD of the retroreflected plane wave is 0.033 λ at $\lambda = 632.8$ nm. The diameter of the null lens is 0.7 cm.

Holleran (1963, 1964) described a null test for concave conicoids that has the virtue that no auxiliary optical elements need be manufactured. The surface to be tested is made level and is immersed in a liquid that forms a planoconvex lens in contact with the surface under test. In the simplest form of the test, a pinhole light source and knife edge are placed at a distance d above the plane surface of the liquid. For liquid lens of thickness t and refractive index n,

$$d = \frac{R}{n} - t \tag{12.34}$$

where R is the vertex radius of curvature of the conicoid. The retroreflected image is corrected for third-order spherical aberration if

$$n^2 = 1 - \frac{KR}{R - t} \tag{12.35}$$

where K is the conic constant of the mirror.

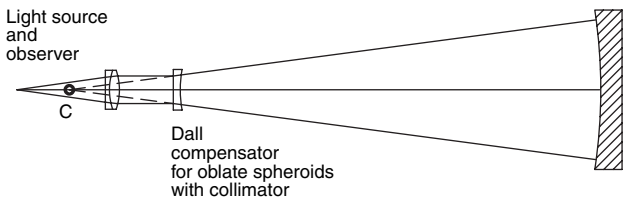

FIGURE 12.41. Compensator for oblate spheroid used with a collimator.

The accuracy of the test is very good for shallow curves of moderate aperture. The peak-to-valley departure ΔW of the surface from the desired conicoid when Eq. (12.29) is satisfied and $t \ll R$ is

$$\Delta W \approx \frac{KR}{41.5\eta^6} \quad \text{waves} \tag{12.36}$$

In Eq. (12.30), η is the f number of the conicoidal mirror, R is its radius in millimeters, and the wavelength is 632.8 nm. The peak-to-valley error of a 0.5-m-diameter $f/3$ paraboloid figured to give a perfect null by this test is 0.10 wave. Decreasing the f number to 2.5 for a mirror having the same aperture increases the figure error to 0.25 wave. The error of an $f/2.5$ mirror reaches 0.10 wave for an aperture of 0.2 m.

The immersion test in this form can also be applied to convex aspherics by observing them through a plane back surface. In this case the optical material replaces the immersion liquid. Puryayev (1971) analyzed an extension of this method in which an immersion fluid is placed above the plane surface. Since the liquid must extend to the retro-reflected image, this extension is practical only for small elements. Puryayev's equations reduce to those of Holleran when the immersion fluid is air.

A related test for convex hyperboloids, described by Norman (1957), makes use of the fact that a planoconvex lens forms a stigmatic image of a collimated source on its axis if the convex surface is a conicoid with eccentricity equal to the refractive index of the material of which the lens is made. The autocollimated image of a point source at a distance of one focal length from the convex surface of lens and reflected from its plane surface, or from a flat mirror parallel to its plane surface, can then be examined to determine the figure of the convex surface. As in the Holleran and Puryayev tests, the range of conicoids that can be tested by this method is limited by the range of refractive indices available. The test can be applied to hyperboloids with magnifications between 3.5 and 5 when the range of glass indices is restricted to 1.5 to 1.8. Holleran (1966) showed that a spherical back surface can provide a null test compensator for a concave oblate spheroid when the latter is tested from the back, through the spherical surface.

12.11. INTERFEROMETERS USING REAL HOLOGRAMS

Many different experimental setups can be used for the holographic testing of optical elements. Because a hologram is simply an interferogram with a large tilt angle between the reference and object wavefronts, holographic tests can be performed either with standard interferometers or with setups having a larger angle between the object and reference beams. Figures 12.42 and 12.43 show interferometers that can be used with a hologram for testing of a concave mirror.

The hologram is made in a plane conjugate to the test mirror. Once the hologram is made, it can be replaced in the same location and reconstructed by illuminating with a plane wave and by imaging onto a viewing screen. When the object beam is blocked and the reference mirror is tilted so that the plane reference wave interferes with the

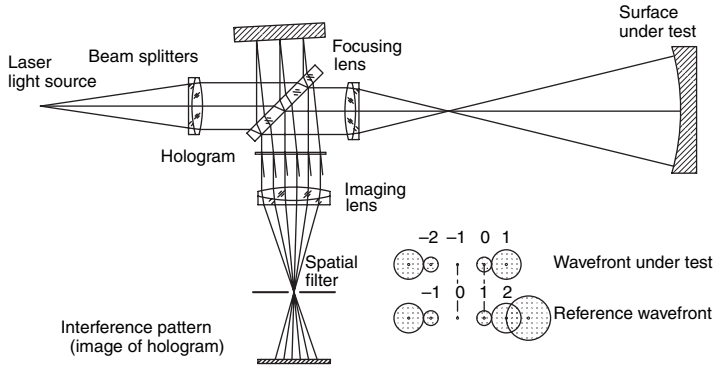

FIGURE 12.42. Twyman–Green interferometer with a holographic compensator.

first-order diffraction from the hologram, the wavefront due to the mirror will be reconstructed. Because several diffraction orders are produced by the hologram, it is usually necessary to select one of the diffraction orders using a spatial filter. The imaging lens and spatial filter are necessary only for the reconstruction of the hologram.

Holograms can be recorded on photographic plates, thermoplastic materials, or in photorefractive crystals. Photographic plates provide the highest resolution; however, they require a lot of chemicals for processing and unless they are processed in situ, they are hard to replace in the correct location for real-time techniques (Biedermann, 1975). Thermoplastic materials provide up to 1000 lines/mm resolution and can be erased and reprocessed hundreds of times (Leung et al., 1979; Friesem et al., 1980). They also have a very fast turnaround time. Photorefractive crystals have a lot of potential as a high-resolution recording medium (Lam et al., 1984; Uhrich and Hesselink 1988); however, the optical setup is more complex, and getting a high-quality crystal is not as easy as getting other recording materials. A very promising recording medium is the use of high-resolution detector arrays or charge-coupled device (CCD) cameras to record a hologram directly.

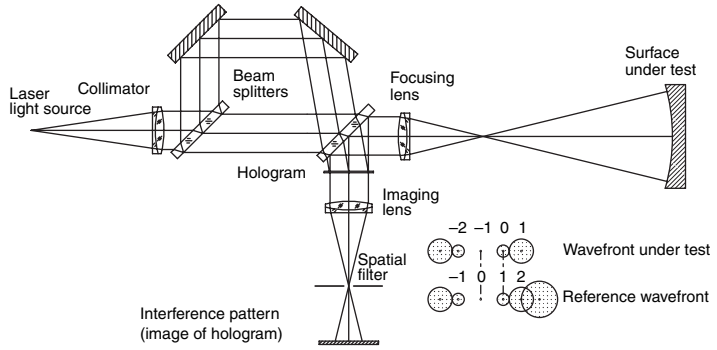

FIGURE 12.43. Mach–Zehnder interferometer with a holographic compensator.

12.11.1. Holographic Wavefront Storage

Sometimes it is convenient to holographically store a wavefront produced by an optical system and analyze the wavefront later without the test system present (Hildebrand et al., 1967; Hansler, 1968).

Q4

Care must be taken to ensure that the reconstructed wavefront is identical to the wavefront used to record the hologram. Errors are possible from differences between the reconstructing geometry and the recording geometry, recording material deformation, and aberrations introduced by the recording-material substrate. Errors introduced because of the differences in the recording and reconstructing geometries are greatly reduced if the reference wavefront is collimated and the object wavefront is collimated as well as possible. Collimated wave fronts are particularly important if the reconstruction wavelength is different from the recording wavelength. Recording-material deformation can change the shape of the recorded interference fringes and thereby change the shape of the reconstructed wavefront. It is possible to keep the root-mean-square (rms) wavefront error less than $\lambda/40$ by using Kodak 649F photographic plates (Wyant and Bennett 1972). Glass substrates used for photographic plates generally show optical-thickness variations of at least one fringe per inch. For wavefront storage, this magnitude of error is not acceptable. This problem can be solved by either putting the hologram in a fluid gate or index matching the two surfaces to good optical flats. Thickness variations can also be minimized by sending both beams through the hologram to cancel the errors.

Stored holograms can be used to test for symmetry in optical components (Greivenkamp, 1987). A hologram is made of the test surface, and then the test surface is rotated with respect to the hologram. The fringes from the interference between the stored wavefront and the wavefront produced by the rotated test surface will correspond to symmetry deviations in the test surface. Care must be taken not to translate the test surface while it is rotated because unwanted fringes will affect the test.

12.11.2. Holographic Test Plate

If an ideal optical system is available, the wavefront produced by the system can be stored holographically and used to test other optical systems. This is very similar to the use of a test plate in the testing of optical components (Hansler, 1968; Pastor, 1969; Snow and Vandewarker, 1970; Lurionov et al., 1972; Broder-Bursztyn and Malacara, 1975). After processing the hologram, it is placed in its original position and the master mirror is replaced with a test mirror. The wavefront stored in the hologram is interferometrically compared with the wavefront produced by the mirror under test. The secondary interference between the stored wavefront and the test wavefront should be recorded in a plane conjugate to the exit pupil of the test surface. If the hologram is made in a plane conjugate to the exit pupil of the mirror under test, the amount of tilt in the resulting interferogram can be selected by simply changing the tilt of the wavefront used in the hologram reconstruction process. If the hologram is not made in a plane conjugate to the exit pupil of the test surface, tilting the reference beam

not only adds tilt to the interferogram, it also causes a displacement between the image of the exit pupil of the test surface and the exit pupil stored by the hologram.

The holographic test plate interferometer can also be thought of in terms of moire patterns (Pastor, 1969). Interference fringes, resulting from the wavefront stored in the hologram and the wavefront coming from the optics under test, can be regarded as the moire pattern between the interference fringes recorded on the hologram plate (formed by the wavefront produced by the master optics and a plane wave) and the real-time interference fringes formed by the wavefront under test and a plane wavefront. The contrast in this moire pattern is increased with spatial filtering by selecting only the wavefront produced by the mirror under test and the diffraction order from the hologram, giving the stored wavefront produced by the master optics.

In addition to the error sources already mentioned, there can be error due to improper positioning of the hologram in the interferometer. Any translation or rotation of the hologram will introduce error. If the hologram is made conjugate to the exit pupil of the master optical system, the exit pupil of the system under test must coincide with the hologram. If the test wavefront in the hologram plane is described by the function $\phi(x, y)$, a displacement of the hologram by a distance Δx in the x direction produces an error

$$\Delta\phi(x,y) \approx \frac{\partial\phi(x,y)}{\partial x}\Delta x \tag{12.37}$$

where $\partial\phi/\partial x$ is the slope of the wavefront in the x direction. Similarly, for a wavefront described by $\phi(r,\theta)$, the rotational error $\Delta\theta$ is given by

$$\Delta\phi(r,\theta) \approx \frac{\partial\phi(r,\theta)}{\partial\theta}\Delta\theta \tag{12.38}$$

Phase-shifting techniques can be used to measure the phase of the secondary interference fringes by placing a phase shifter in the reference beam of the interferometer and shifting the phase of the secondary interference fringes (Hariharan et al., 1982; Hariharan, 1985). Because the secondary interference fringe spacing corresponds to one wavelength of OPD between the stored wavefront and the live test surface wavefront, a $\pi/2$ phase shift of the fringes for the test surface will cause a $\pi/2$ phase shift in the secondary interference fringes. The calculated phase surface will correspond to the difference between the master optical component and the test optical component. To ensure that the fringes actually correspond to the test surface, the hologram must be made in the image plane of the test surface, and the hologram plane must be imaged onto the detector array when the phase measurement is performed.

12.12. INTERFEROMETERS USING SYNTHETIC HOLOGRAMS

When master optics are not available to make a real hologram, a computer generated (or synthetic) hologram (CGH) can be made (Pastor, 1969; Lee, 1970,1974;

MacGovern and Wyant, 1971; Wyant and Bennett, 1972; Schwider and Burow, 1976; Caulfield et al., 1981; Ono and Wyant, 1984; Dörband and Tiziani, 1985; Beyerlein et al., 2002; Reichelt et al., 2004; Pruss et al., 2004). A CGH is a binary representation of the actual interferogram (hologram) that would be obtained if the ideal wavefront from the test system is interfered with a tilted plane wavefront. The test setup is the same as that for a real hologram used as a holographic test plate. CGHs are an alternative to null optics when testing aspheric optical components.

12.12.1. Fabrication of Computer-Generated Holograms (CGHs)

To make a CGH, the test setup must be ray traced to obtain the fringes in the hologram plane that result from the interference of the tilted plane wave and the wavefront that would be obtained if the mirror under test were perfect. Just like a real hologram used as a test plate, the CGH should be made in a plane conjugate to the exit pupil of the system under test. These fringes are then represented as a binary grating, commonly having a 50% duty cycle. Methods for calculating these fringes are outlined by Wyant and Bennett (1972), Lee (1974), and Arnold (1989). A procedure that encodes the fringes as a series of exposure rectangles is discussed by Leung et al., (1980). The process of breaking fringes into rectangles or polygons reduces the amount of computer storage necessary and the time needed to plot the CGH. The procedure used to make a CGH can be employed for any general optical system as long as all the optics in the interferometer are known and can be ray traced.

A typical CGH is shown in Figure 12.44. An example of an interferometer used to test a steep aspheric optical element is shown in Figure 12.45. If the deviation of the test surface from a sphere is substantial, the marginal rays (not the paraxial rays) will follow a different path back through the divergent lens after they have reflected off the test surface. When the surface under test is properly imaged at the observation

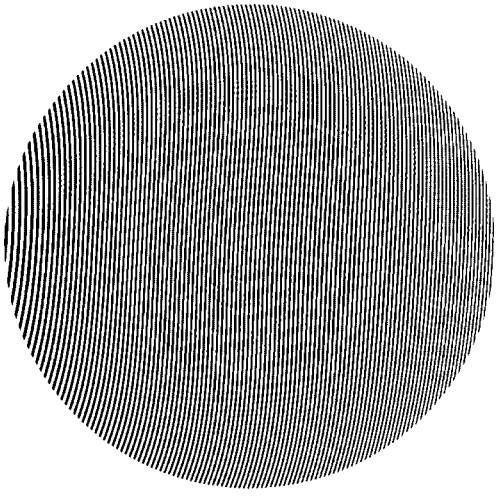

FIGURE 12.44. Computer generated hologram.

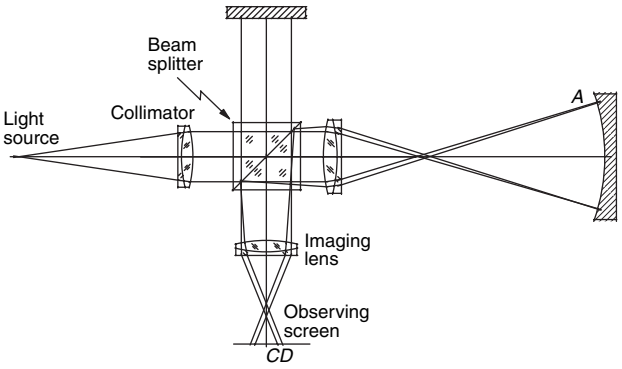

FIGURE 12.45. Aspheric test surface in interferometer showing rays not following same path after reflection off the test surface.

plane, the marginal rays will arrive at the observation plane at the same point where the corresponding ray following the path through the reference mirror arrives, as when there is no aspherical deformation, even if the path followed by the ray is different. By Fermat's principle, the optical path from any point on the surface under test to the observation plane is the same for all possible paths, automatically correcting the error. In conclusion, when there is no proper imaging of the surface being tested over the detector, there will be an additional aberration added to the final interferogram. However, in this case, when the entire system is ray traced, the hologram can be designed to correct these extra aberrations if a null test is performed. Another important consideration is that the test element may deviate the rays so much that the light reflected from the test surface will not get back through the interferometer. In this case, a partial null lens must be used to ensure that light will get back through the system. This is discussed in more detail in the section on the combination of CGHs with null optics.

Once the fringes are calculated, they are either plotted directly on a holographic substrate, or plotted and photographically reduced onto a holographic substrate. The techniques of plotting have been substantially improved over the years. Early work utilized pen plotters to make an enlarged version of the hologram that was then photographically reduced to the appropriate size (MacGovern and Wyant, 1971; Wyant and Bennett, 1972; Wyant et al., 1984; Wyant and O'Neill, 1974). The large format enabled a high-resolution CGH to be formed. However, problems due to plotter irregularities such as line thickness, pen quality, plotter distortion, and quantization caused errors in the reconstructed wavefront. Nonlinearities inherent in the photographic process and distortion in the reduction optics caused further degradation. With the advent of laser-beam recorders, resolution improved due to machine speed and an increased number of distortion-free recording points (Wyant et al., 1984). The most recent advances in the recording of CGHs have been made using the electron beam (e-beam) recorders used for producing masks in the semiconductor industry (Emmel and Leung, 1979; Leung et al., 1979, 1980; Arnold, 1989). These machines write onto photoresist deposited on an optical quality glass plate and currently produce the

highest quality CGHs. Patterns with as many as 108 data points can be produced in a hologram of the desired size. Typical e-beam recorders will write a 1-mm area with a resolution of 0.25 μm. Large patterns are generated by stitching a number of 1-mm scans together. Errors in this technique are due to aberrations in the electron optics, beam drift, instabilities in the controlling electronics, and positioning of the stepper stage. For in-line holograms a thermochemical method with selective oxidation of a Cr coated substrate has been used by Burge et al. (1994). Then, a special writing machine with a rotary air-bearing spindle rotates the substrate to selectively oxidize some rings with an Ar^+ laser. After writing the pattern, the substrate with its coating is immersed in a liquid that removes all non oxidized Cr.

Many of the errors in CGHs are reproducible and can be compensated for in the software controlling the recorder (Chang and Burge 1999 and Arnold and Kestner 1995). Plotter errors can be evaluated by generating a hologram that is composed of straight lines in orthogonal directions forming a grid (Wyant et al., 1984). This test hologram is then illuminated with two plane waves as shown in Figure 12.46 to interfere the $+N$ and $-N$ orders. Deviations of the fringes from straight lines will correspond to errors in the plotting process. The resulting aberration in the interferogram is $2N$ times that of the first order.

12.12.2. Using a CGH in an Interferometer

A CGH test is performed by interfering the test wavefront with a reference wavefront stored in the hologram. This entails overlapping the zero-order test beam and the first-order reference beam from the hologram in the Fourier plane of the hologram. The test can also be performed by interfering the minus first-order test beam with the zero-order reference beam to compare the two plane waves instead of the two aspheric wavefronts. When the test wavefront departs from the reference wavefront, fringes corresponding to the difference between the wavefronts appear. In the Fourier plane of the hologram, the zero- and first-order diffracted spots of the reference wavefront will overlap the minus first- and zero-order diffracted spots of the test wavefront when the interferometer is correctly aligned. Both outputs yield the same interferogram. Spatial filtering can be used to improve the fringe contrast if the tilt of the plane reference wavefront used for the hologram is large enough.

The CGH compensator can be used off axis as well as in line, with different advantages and disadvantages, as we will show in the next sections.

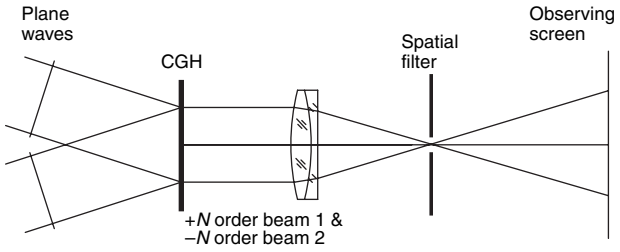

FIGURE 12.46. Test setup with $\pm N$ orders of hologram interfering to test the quality of a CGH plotter.

Also, the position where the CGH is located can be different. There are two possibilities, one is to place the hologram in the testing space where only the wavefront under test passes through the hologram. A second possibility is to place it in the observation space, where both interfering wavefronts pass through the hologram. Let us analyze these two cases with some detail. A CGH is sensitive to the same errors as real holograms. Because of this, the CGH should be placed in the interferometer, so that thickness variations in the hologram substrate have no effect on the results. The importance of this will depend on where the CGH is located.

(a) If the hologram is placed in the observation space, both the reference wavefront and the wavefront under test pass through the hologram. Each wavefront generates its own diffracted wavefronts. Proper spatial filtering should be performed so that the interference pattern is generated with the diffracted reference wavefront (aspheric) and the wavefront under test or with the nondiffracted reference wavefront (flat) and the compensated wavefront under test (nearly plane). Since the CGH is traversed by both interfering wavefronts, any small imperfection in the glass plate of the CGH is unimportant.

In this case, the superposition of the hologram and the interference pattern can be considered as a Moiré pattern. If this pattern is spatially filtered, the interferogram representing the wavefront deviations with respect to the aspheric surface (not with respect to a plane) is obtained. If desired, this procedure can even be carried out by the superposition of two transparencies of the interferogram and the hologram, as illustrated in Figure 12.47.

(b) If the hologram is placed in the interferometer test space only the wavefront under test will pass through the hologram, but it will pass twice through it. Let us represent the diffracted beams after the first pass by their order of diffraction number ($\ldots -2, -1, 0, 1, 2 \ldots$). Since all these beams come back to the hologram after reflection on the aspheric surface under test, they can now be represented by a pair of numbers, the first one being the order of diffraction on the first pass and the second one the order of diffraction on the second pass. These beams are ordered as follows:

$$
\begin{array}{ccccc}
(-1,-1) & (-1,0) & (-1,1) & & \\
 & (0,-1) & (0,0) & (0,1) & \\
 & & (1,-1) & (1,0) & (1,1)
\end{array}
$$

Each column here corresponds to a different diffracted angle. Proper spatial filtering should then be performed to isolate and observe only the desired beams, for example (1, 0) with (0, −1) or (0, 1) with (1, 0). Since only the wavefront under test passes through the hologram, the CGH must be made in a good glass plate, with flat faces and homogeneous refractive index, otherwise its aberrations will be added to the diffracted wavefronts.

In addition to the error sources associated with a real hologram, a CGH has additional error sources due to plotter distortion, incorrect hologram size, and photoreduction distortion if the hologram is photographically reduced in size. These

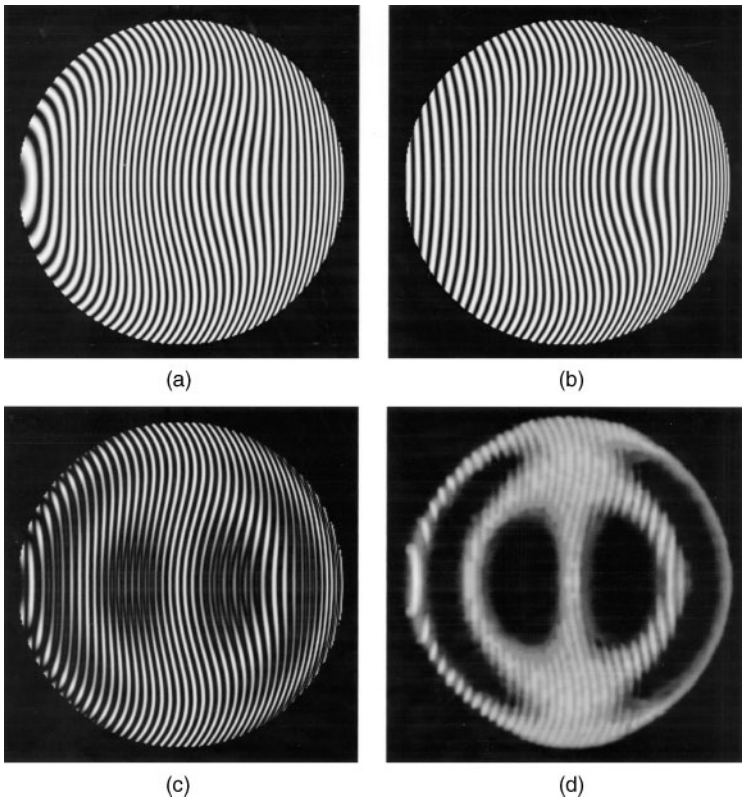

FIGURE 12.47. Moiré analysis of an interferogram with a large tilt (linear carrier). (a) Interferogram to be analyzed, (b) ideal computer generated interferogram, (c) superposition of the interferogram with the ideal reference interferogram and, (d) low pass filtered interferogram combination.

errors are proportional to the maximum slope of the departure of the test wavefront from a spherical or plane wavefront. These errors can be minimized when the test wavefront is calculated relative to the spherical wavefront, which minimizes the slope of the test wavefront departure from a spherical wavefront. Errors due to photographic reduction can be eliminated by writing a hologram of the correct size directly onto a glass substrate using an e-beam recorder.

One source of error is incorrect hologram size. If the aberrated test wavefront in the plane of the hologram is given by $\phi(r, \theta)$, a hologram of incorrect size will be given by $\phi(r/M,\theta)$, where M is a magnification factor. The error due to incorrect hologram size will be given by the difference $\phi(r/M, \theta) - \phi(r, \theta)$ and can be written in terms of a Taylor expansion as

$$\begin{aligned}\phi\left(\frac{r}{M},\theta\right) - \phi(r,\theta) &= \phi\left[r + \left(\frac{1}{M} - 1\right)r, \theta\right] - \phi(r,\theta) \\ &= \left[\frac{\partial\phi(r,\theta)}{\partial r}\right]\left(\frac{1}{M} - 1\right)r + \cdots\end{aligned} \tag{12.39}$$

where terms higher than first order can be neglected if M is sufficiently close to 1 and a small region is examined. Note that this error is similar to a radial shear. When the CGH is plotted, alignment aids, which can help in obtaining the proper hologram size, must be drawn on the hologram plot.

The largest source of error is distortion in the hologram plotter (Wyant et al., 1984). The CGH wavefront accuracy depends on the number of plotter resolution points and the maximum slope of the aspheric wavefront being tested. Assuming that the plotter has $P \times P$ resolution points, there are $P/2$ resolution points across the radius of the hologram. Since the maximum error in plotting any point is half a resolution unit, any portion of each line making up the hologram can be displaced by a distance equal to $1/P$. If the maximum difference between the slope of the test wavefront and the tilted plane wave is $4S$ waves per hologram radius, the phase of the plane wave at the hologram lines can differ from that of the required wavefront at the same lines by as much as $4S/P$ waves (1980). The maximum error in the reconstructed wavefront will be $4S/P$ waves, and since the final interferogram is recorded in the image plane of the hologram, the quantization due to the finite number of resolution points causes a peak error in the final interferogram of $4S/P$ waves. It is important to note that the peak wavefront error of $4S/P$ waves is really a worst-case situation; it occurs only if, in the region of the hologram where the slope difference is maximum, the plotter distortion is also a maximum. This systematic error due to plotter distortion can be calibrated when the plotter distortion is known (Wyant et al., 1984). When the maximum plotting error is equal to one-half of the resolution spot size, the sensitivity of the CGH test ΔW is given by $4S/P$, where P is the number of distortion-free plotter points. Using an e-beam recorder with 0.25-μm resolution over a l0-mm-diameter hologram would enable the measurement of an aspheric wavefront with a maximum wavefront slope of 1000 waves per radius to be tested to a sensitivity of $\lambda/10$ (assuming a perfect plotter).

Q5

12.12.3. Off-Axis CGH Aspheric Compensator

To ensure that there is no overlapping of the first and second orders in the Fourier plane (where the spatial filter is located), the tilt angle of the reference plane wave needs to be greater than three times the maximum wavefront slope of the aberrated wave. (Note that there are no even orders for a grating with a 50% duty cycle.) A photograph of the diffracted orders from the hologram in the Fourier plane is shown in Figure 12.48, and a diagram detailing the necessary separations of the orders in the Fourier plane is shown in Figure 12.49. The bandwidth of the N^{th} order is given by $2NS$, where S is the maximum wavefront slope in waves per radius of the wavefront to be reconstructed. This bandwidth (diameter of the diffracted beam in the Fourier plane) determines the size of the spatial-filtering aperture. By moving the spatial-filtering aperture, the output of the interferometer can either be the interference of two plane waves or two aspheric waves.

If the hologram is recorded on a very high-quality optical flat or used in reflection, it can be placed in a single beam of the interferometer, as illustrated in Figure 12.50 using a Fizeau configuration. As we mentioned before, with a pinhole we can isolate,

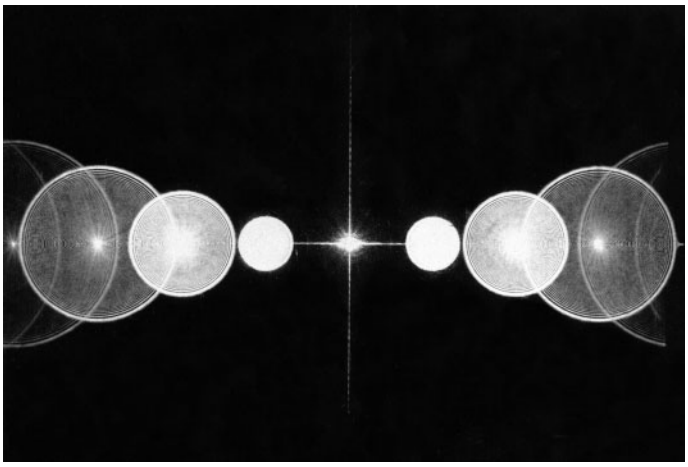

FIGURE 12.48. Diffracted order in Fourier plane of CGH.

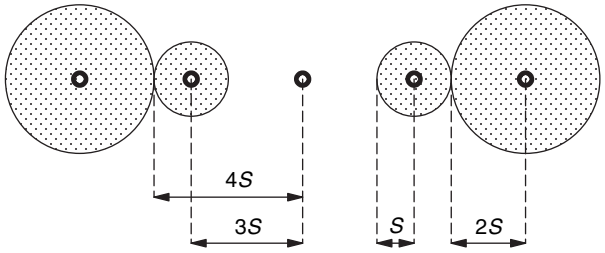

FIGURE 12.49. Diffracted orders in Fourier plane of CGH.

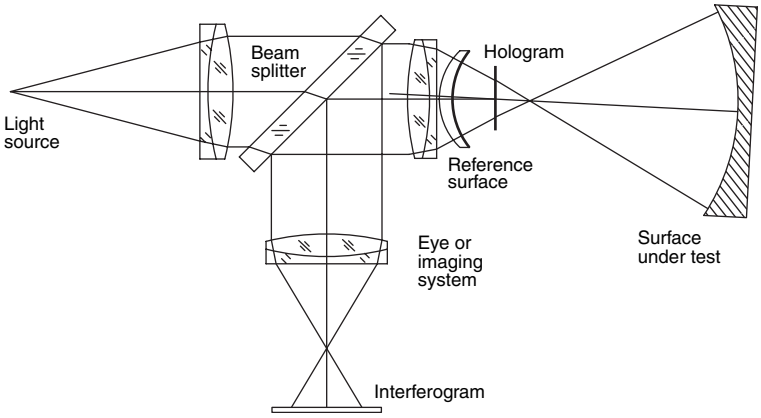

FIGURE 12.50. Fizeau interferometer utilizing a CGH in one beam.

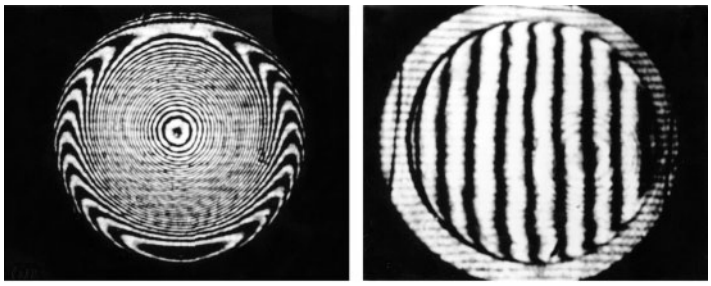

FIGURE 12.51. Results of testing a 10-cm diameter *F*/2 paraboloid (a) without and (b) with a CGH made using an e-beam recorder.

either the diffracted orders $(-1, 0)$ with $(0, -1)$ or the orders (0,1) with (1,0). The whole wavefront compensation is performed in only one of the two passes through the CGH.

Figure 12.50 shows the results of measuring a l0-cm-diameter F/2 parabola using a CGH generated with an e-beam recorder (Leung et al., 1980). The fringes obtained in a Twyman–Green interferometer using a helium–neon source without the CGH present are shown in Figure 12.51(a). After the CGH is placed in the interferometer, a much less complicated interferogram is obtained as shown in Figure 12.51(b). The CGH corrects for about 80 fringes of spherical aberration and makes the test much easier to perform.

12.12.4. In-Line CGH Aspheric Compensator

In-line CGHs have the disadvantage with respect to off-axis CGHs that high-order images cannot be completely separated. In this hologram, the separation is made taking advantage that they are focused at different planes, but the isolation of the desired first order cannot be complete. However, they have two great advantages. First, that the alignment is much simpler and second, that since the lateral carrier is not introduced, the degree of asphericity that can be measured is higher. In-line CGH compensators have been described by Mercier et al., (1980), Fercher (1976), and Tiziani et al. (2001). They can be used in a Twyman–Green or Fizeau interferometer, as shown in Figure 12.52.

To avoid asymmetry, so that the paths in and out of the system formed by the CGH and surface under test are the same, the beam to be isolated to produce the interference pattern with the reference beam is the (1, 1).

To test an aspheric convex surface, the arrangement shown in Figure 12.53 can be used. However, to reduce the required size of the auxiliary reference concave surface, the separation between the reference surface and the convex surface can be reduced to a small distance, as suggested by Burge (1995), by engraving the hologram rings on the concave reference surface, as illustrated in Figure 12.54. Notice that the light rays arrive perpendicularly to the concave reference surface, and then, after diffraction, they become perpendicular to the surface under test. Thus, even if the reference

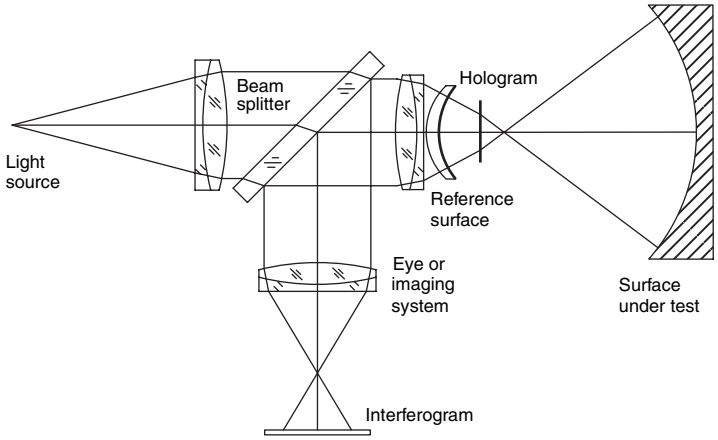

FIGURE 12.52. Testing a concave aspheric surface with an in-line CGH compensator used in a Fizeau interferometer.

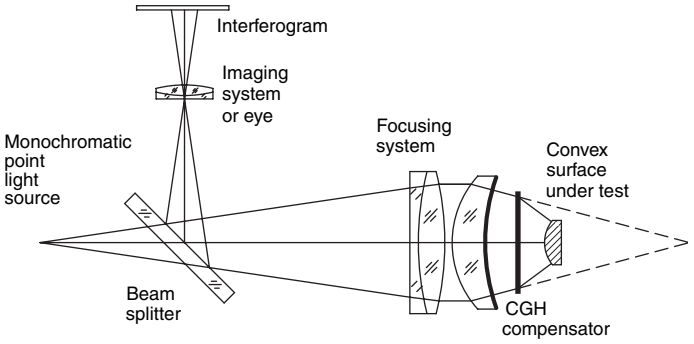

FIGURE 12.53. Testing a convex aspheric surface with an in-line CGH compensator used in a Fizeau interferometer.

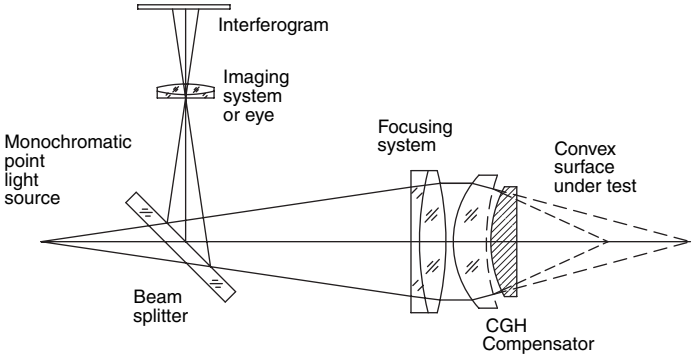

FIGURE 12.54. Testing a convex aspheric surface with a test plate with an in-line CGH compensator on its concave surface.

surface and the surface under test are placed in contact at the vertex, they would not have exactly the same curvature.

12.12.5. Combination of CGH with Null Optics

Although a CGH can be designed for any optical system, a point is reached where the time and expense required to make a CGH are unreasonable. Also, given enough time and money, null optics, either reflective or refractive, can be designed and built to test almost any arbitrarily complicated optical system.

It is possible to replace the complicated CGH or the complicated null optics required to test complicated optical surfaces (notably aspherical surfaces) with a combination of relatively simple null optics and a relatively simple CGH.

To illustrate the potential of the combined test, results for a CGH-null-lens test of the primary mirror of an eccentric Cassegrain system with a departure of approximately 455 waves (at 514.5 nm) and a maximum slope of approximately 1500 waves per radius are shown in Figure 12.55 (Wyant and O'Neill, 1974). The mirror was a 69-cm-diameter off-axis segment whose center lies 81 cm from the axis of symmetry of the parent aspheric surface. The null optics was a Maksutov sphere (as illustrated in Figure 12.56), which reduces the departure and slope of the aspheric wavefront

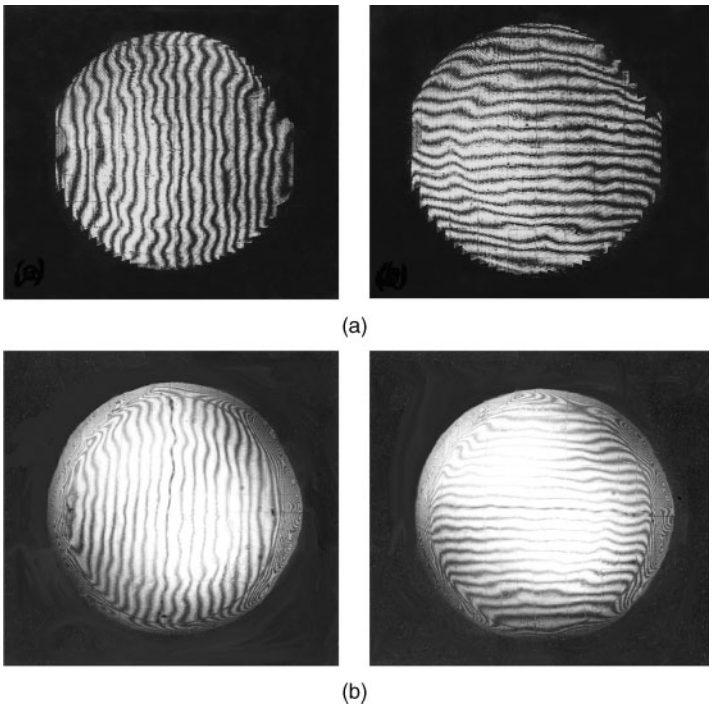

FIGURE 12.55. Setup to test the primary mirror of a Cassegrain telescope using a Maksutov sphere as a partial null with a CGH.

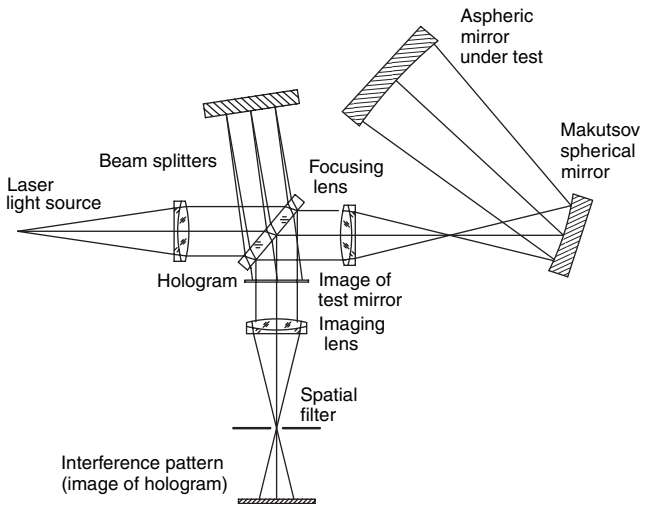

FIGURE 12.56. Results of testing using setup of Figure 12.55 (a) CGH-Maksutov test ($\lambda = 514.5$ nm) and using null lens ($\lambda = 632.8$ nm). (From Wyant and O'Neill, 1974.)

from 910 to 45 waves and from 3000 to 70 waves per radius, respectively. A hologram was then used to remove the remaining asphericity.

Figure 12.55(a) shows interferograms obtained using the CGH-Maksutov test of the mirror under test. Figure 12.55(b) shows the results when the same test was performed using a rather expensive refractive null lens. When allowance is made for the fact that the interferogram obtained with the null lens has much more distortion than the CGH-Maksutov interferogram, and for the difference in sensitivity ($\lambda = 632.8$ nm for the null lens test and 514.5 nm for the CGH-Maksutov test), the results for the two tests are seen to be very similar. The ''hills'' and ''valleys'' on the mirror surface appear the same for both tests, as expected. The peak-to-peak surface error measured using the null lens was 0.46 waves ($\lambda = 632.8$ nm), while for the CGH-Maksutov test it was 0.39 waves (514.5 nm). The rms surface error measured was 0.06 waves (632.8 nm) for the null lens, while the CGH-Maksutov test gave 0.07 waves ($\lambda = 514.5$ nm). These results certainly demonstrate that expensive null optics can be replaced by a combination of relatively inexpensive null optics and a CGH.

The difficult problem of testing aspheric surfaces, which are becoming increasingly popular in optical design, is made easier by the use of CGHs. The main problem with testing aspheric optical elements is reducing the aberration sufficiently to ensure that light gets back through the interferometer. Combinations of simple null optics with a CGH to perform a test enable the measurement of almost any optical surface. The making and use of a CGH are analogous to using an interferometer setup that yields a large number of interference fringes and measuring the interferogram at a large number of data points. Difficulties involved in recording and analyzing a high-density interferogram and making a CGH are very similar. In both cases, a large

number of data points are necessary, and the interferometer must be ray traced so that the aberrations due to the interferometer are well known. The advantage of the CGH technique is that once the CGH is made, it can be used for testing a single piece of optics many times or for testing several identical optical components (Greivenkamp, 1987). In addition, it is much easier for an optician to work with a null setup.

12.13. ASPHERIC TESTING WITH TWO-WAVELENGTH HOLOGRAPHY

The surface under test is often not known close enough to perform a null test. Even if a null test is attempted, the resulting interferogram may contain too many fringes to analyze. Since high accuracy may not be needed, a longer wavelength light source could be used in the interferometer to reduce the number of fringes. Unfortunately, a long wavelength light source creates problems because film and detector arrays may not be available to record the interferogram directly, and the inability to see the radiation causes considerable experimental difficulty. Two-wavelength and multiple-wavelength techniques provide a means of synthesizing a long effective wavelength using visible light to obtain an interferogram identical to the one that would be obtained if a longer wavelength source were used as shown by several authors, among others by Wyant (1971); Wyant et al. (1984); Cheng and Wyant (1984, 1985); Creath et al. (1985); Creath and Wyant (1986); and Wyant and Creath (1989).

Two-wavelength holography is performed by first photographing the fringe pattern obtained by testing an optical element using a wavelength λ_1 in an interferometer such as the interferometer shown in Figure 12.56. This photographic recording of the fringe pattern (hologram) is then developed, replaced in the interferometer in the exact position it occupied during exposure, and illuminated with the fringe pattern obtained by testing the optical element using a different wavelength λ_2. The resulting two-wavelength fringes can either be thought of as the moire between the interference fringes stored in the hologram (recorded at λ_1 and replayed at λ_2) and the live interference fringes (at λ_2), or as the secondary interference between the test wavefront stored in the hologram and the live test wavefront. These fringes are identical to those that would be obtained if the optical element was tested using a long effective wavelength given by (Wyant, 1971)

$$\lambda_e = \frac{\lambda_1 \lambda_2}{|\lambda_1 - \lambda_2|} \tag{12.40}$$

Table 12.6 lists the values of λ_e that can be obtained using various pairs of wavelengths from an argon-ion and a helium–neon laser. By the use of a dye laser, a large range of equivalent wavelengths can be obtained. Tunable helium–neon lasers with four or five distinct wavelengths ranging from green to red are also available.

The contrast in the final interferogram can be increased by spatial filtering. If the filtering is to be effective, the angle between the two interfering beams in the interferometer must be such that only the object beam, not the reference beam,

TABLE 12.6. Possible effective wavelengths in μm obtainable with argon–ion and helium–neon lasers.

λ in nm	459.7	476.5	488.0	496.5	501.7	514.5	632.8
459.7	—	11.73	9.95	5.89	5.24	4.16	1.66
476.5	11.73	—	20.22	11.83	9.49	6.45	1.93
488.0	9.95	20.22	—	28.50	17.87	9.47	2.13
496.5	5.89	11.83	28.50	—	47.90	14.19	2.30
501.7	5.24	9.49	17.87	47.90	—	20.16	2.42
514.5	4.16	6.45	9.47	14.19	20.16	—	2.75
632.8	1.66	1.93	2.13	2.30	2.42	2.75	—

passes through the spatial filter (aperture) shown in Figure 12.56. The spatially filtered pattern yields the interference between the wavefront produced by illuminating (with wavelength λ_2) the hologram recorded at wavelength λ_1 and the wavefront obtained from the optical element using wavelength λ_2. Since the two-wavelength holography interferogram provides the difference between the two interfering beams only in the plane of the hologram, the fringe pattern (hologram) must be recorded in the plane conjugate to the test surface. The final photograph of the interferogram should be recorded in the image plane of the hologram.

Figure 12.57(a) shows an interferogram of an optical element tested using a wavelength of 488.0 nm. The other interferograms were obtained using two-wavelength holography to test the same optical element. The interferograms in Figures 12.57(b) to 12.57(e) were obtained by recording an interferogram (hologram) using a wavelength of 514.5 nm and illuminating the recording with the fringe pattern obtained using a wavelength of 476.5 nm for Figures 12.57(b,c) and of 488.9 nm for Figures 12.57(d,e). The interferograms were spatially filtered, and the amount of tilt shown was adjusted in real time by changing the angle at which the reference wavefront was incident on the hologram during the reconstruction. The
Q6 interferograms in Figures 12.57(f,g) were obtained by recording an interferogram using a wavelength of 488.0 nm and illuminating this recording with the fringe pattern obtained using a wavelength of 476.5 nm and of 496.5 nm, respectively.

In two-wavelength holography, the final interferogram gives the difference between a fringe pattern recorded at one instant of time and a fringe pattern existing at some later instant of time. If the two fringe patterns are different for reasons other than wavelength change (e.g., air turbulence), incorrect results are obtained. This means that if air turbulence causes a one-fringe change between the fringe pattern obtained using $\lambda_1 = 488.0$ nm and the fringe pattern obtained using $\lambda_2 = 514.5$ nm, the final interferogram will contain one fringe of error corresponding to 9.47 μm.

The effect of air turbulence can be reduced by simultaneously recording the interferograms resulting from the two wavelengths. If the recording process is sufficiently nonlinear and the interferograms have sufficiently high contrast, the interferogram obtained shows the Moiré pattern described earlier. Generally, this Moiré pattern is too low in contrast to be useful. However, when this interferogram (hologram) is illuminated with a plane wave, is spatially filtered, and is reimaged in

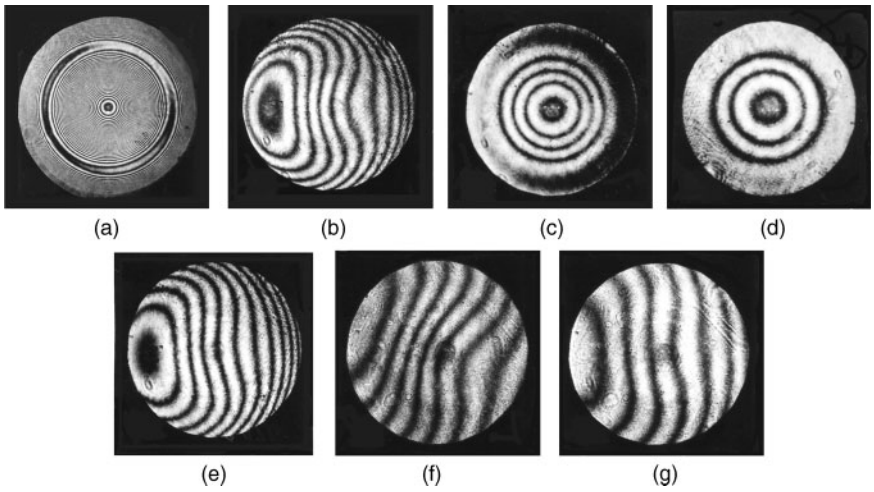

FIGURE 12.57. Interferograms of an aspheric surface with three different defocusing values. The useful ring where the fringes can be processed has a larger contrast than the rest.

the manner shown in Figure 12.56, the result is a high-contrast interferogram, identical to that obtained using the two-wavelength holography method described earlier. Since both fringe patterns are recorded simultaneously, and air dispersion is small, the sensitivity of the interferometer to air turbulence is essentially the same as if a long wavelength light source were used in the interferometer.

More details on the applications of two-wavelength and multiple-wavelength interferometry will be given in Chapter 15.

12.14. WAVEFRONT STITCHING

When the wavefront is strongly aspheric and even with zero tilt in the reference wavefront, the minimum fringe spacing is too small an option to measure the wavefront by segmenting the complete aperture in small regions where the Nyquist condition is not violated, so that the minimum fringe spacing is larger than twice the pixel spacing. There are many approaches to dividing the aperture, but they can be classified in three broad categories.

12.14.1. Annular Zones

One obvious procedure to is to use several different defocussing values, as described by Liu et al. (1988) and by Melozzi et al. (1993). Then, for several rings where the fringe spacing never exceeds, the Nyquist limit are obtained. This is clearly illustrated in Figure 12.58 where three different defocusing values are used. The useful ring where the fringes can be processed has a much larger contrast than the rest.

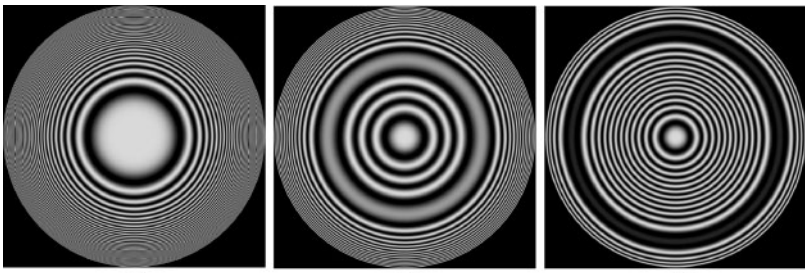

FIGURE 12.58. Schematics of the system to produce a dynamic tilt switching of the reference wavefront in a Mach–Zehnder interferometer.

12.14.2. Circular Zones

Another method to measure an aspherical surface by stitching is to divide the aperture in many circular zones where the tilt as well as the defocusing is optimized to maximize the minimum fringe spacing. For example, the evaluation of an aspheric surface can be made with many small glass test plates, each one optimized for a different region (Jensen et al., 1984).

This method is also useful when measuring large optical surfaces whose size is much larger than the interferometer aperture (Sjödahl and Oreb, 2002), for example, when testing an extremely large plane (Negro, 1984). Special techniques must be used to insure the continuity of the different apertures, for example with some overlapping and polynomial fitting of the apertures to join them.

12.14.3. Dynamic Tilt Switching

Still another approach, described by Liesener and Tiziani (2004) and Liesener et al. (2004), is to change the tilt in a dynamic manner. Here, again, the useful zone has a much better contrast than the undersampled zone, where the fringes cannot be processed.

To change the tilt of the reference wavefront in a Twyman–Green interferometer in a dynamic manner, the arrangement in Figure 12.59 is used, where the tilted reference beam is generated by electronically selecting different point light sources in a rectangular array. This array, called a phase shifting point source array consists of a high resolution liquid crystal display, followed by a microlens array and an array of pinholes in front of it, at the focii of the microlenses. When a small zone in front of a pinhole is made transparent, all the rest are opaque. However, even if all zones are made transparent, the light from a microlens enter a pinhole only if the light passing thorough a diffraction grating generated on the desired zone diffracts the light so that the first order diffracted light falls on the pinhole. This is illustrated in Figure 12.60. Once a tilt has been selected, the interferogram to be processed is like those in Figure 12.61.

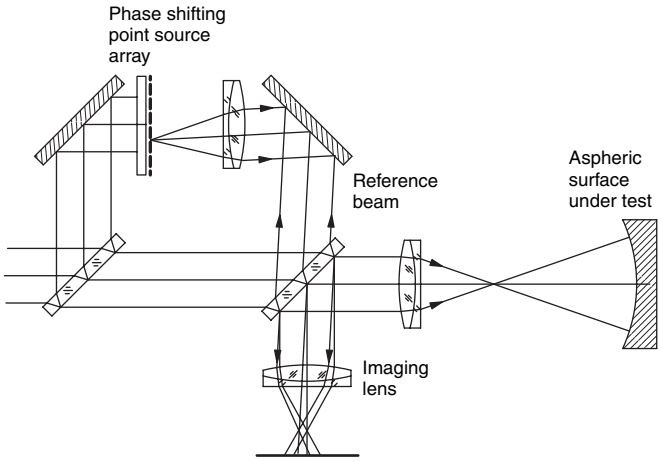

FIGURE 12.59. Detail of the device used to the dynamic tilt switching.

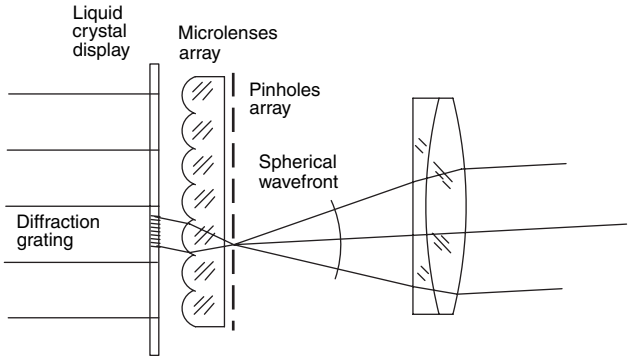

FIGURE 12.60. Interferograms with three different tilts. The zone to be processed is that with the large fringe spacing, not exceeding the Nyquist limit for the detector being used.

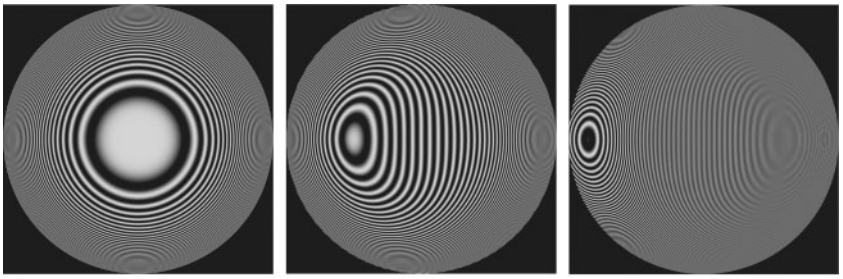

FIGURE 12.61. Interferograms of an optical element at a number of different effective wavelengths: (a) $\lambda = 488\,\text{nm}$, (b) $\lambda_e = 6.45\,\mu\text{m}$, (c) $\lambda_e = 6.45\,\mu\text{m}$, (d) $\lambda_e = 9.47\,\mu\text{m}$, (e) $\lambda_e = 9.47\,\mu\text{m}$, (f) $\lambda_e = 20.22\,\mu\text{m}$, (g) $\lambda_e = 28.50\,\mu\text{m}$. (From Wyant, 1971.)

REFERENCES

Arnold S. M., ''How to Test an Asphere with a Computer-Generated Hologram,'' *Proc. SPIE*, 1052, 191–197 (1989).

Arnold S. M. and R. Kestner, ''Verification and Certification of CGH Aspheric Nulls,'' *Proc. SPIE*, 2636, 117–126 (1995).

Beyerlein M., N. Lindlein, and J. Schwider, ''Dual-Wave-Front Computer-Generated Holograms for Quasi-Absolute Testing of Aspherics,'' *Appl. Opt.*, 41, 2440–3106 (2002).

Biedermann K., ''Information Storage Materials for Holography and Optical Data Processing,'' *Opt. Acta*, 22, 103–124 (1975).

Broder-Bursztyn F. and D. Malacara, ''Holographic Interferometer to Test Optical Surfaces,'' *Appl. Opt.*, 14, 2280–2282 (1975).

Bruns D. G., ''Null Test for Hyperbolic Convex Mirrors,'' *Appl. Opt.*, 22, 12 (1983).

Burch C. R., ''On Reflection Compensators for Testing Paraboloids,'' *Mon. Not. R. Astron. Soc.*, 96, 438 (1936).

Burch C. R., ''Report of the General Meeting of the Association,'' *J. B. Astron. Assoc.*, 48, 99 (1938).

Burge J. H., D. S. Anderson, T. D. Milser, and C. L. Vernold, ''Measurement of a Secondary Mirror Using a Holographic Test Plate,'' *Proc. SPIE*, 2199, 193–198 (1994).

Burge J. H., ''Fizeau Inteferometry for Large Convex Surfaces,'' *Proc. SPIE*, 2536, 127–138 (1995).

Caulfield H. J., P. Mueller, D. Dvore, A. Epstein, and J. S. Loomis, ''Computer Holograms for Optical Testing,'' *Proc. SPIE*, 306, 154–157 (1981).

Chang Y.-C. and J. H. Burge, ''Error Analysis for CGH Optical Testing,'' *Proc. SPIE*, 3782, 358–366 (1999).

Cheng Y.-Y. and J. C. Wyant, ''Two-Wavelength Phase Shifting Interferometry,'' *Appl. Opt.*, 23, 4539–4543 (1984).

Cheng Y.-Y. and J. C. Wyant, ''Multiple-Wavelength Phase Shifting Interferometry,'' *Appl. Opt.*, 24, 804–807 (1985).

Couder A., ''Procede d'Examen d'un Miroir Concave Non-Spherique,'' *Rec. Opt. Theor. Instrum.*, 6, 49 (1927).

Creath K. and J. C. Wyant, ''Direct Phase Measurement of Aspheric Surface Contours,'' *Proc. SPIE*, 645, 101–106 (1986).

Creath K., Y.-Y. Cheng, and J. C. Wyant, ''Contouring Aspheric Surfaces Using Two-Wavelength Phase-Shifting Interferometry,'' *Opt. Acta*, 32, 1455–1464 (1985).

Dall H. E., ''A Null Test for Paraboloids,'' *J. Br. Astron. Assoc.*, 57, 201 (1947).

Dall H. E., ''A Null Test for Paraboloids,'' in *Amateur Telescope Making*, vol. 3, A. E. Ingalls, Ed., Scientific American, New York, 1953, pp. 149–153.

Dörband and H. J. Tiziani, ''Testing Aspheric Surfaces with Computer Generated-Holograms: Analysis of Adjustment and Shape Errors,'' *Appl. Opt.*, 24, 2604–2611 (1985).

Dyson J., ''Unit Magnification Optical System without Seidel Aberrations,'' *J. Opt. Soc. Am.*, 49, 713 (1959).

Emmel P. M., K. M. Leung, ''A New Instrument for Routine Optical Testing of General Aspherics,'' *Proc. SPIE*, 171, 93–99 (1979).

Everhart E., ''Null Test for Wright Telescope Mirrors,'' *Appl. Opt.*, 5, 717–718 (1966).

Friesem A. A., Y. Katzir, Z. Rav-Noy, and B. Sharon, ''Photoconductor-Thermoplastic Devices for Holographic Nondestructive Testing,'' *Opt. Eng.*, 19, 659–665 (1980).

Geary J. M. and L. J. Parker, ''New Test for Cylindrical Optics,'' *Opt. Eng.*, 26, 813–820 (1987).

Geary J. M., ''Fiber/Cylinder Interferometer Test: Focus and Off-Axis Response,'' *Opt. Eng.*, 30, 1902–1909 (1991).

Greivenkamp J. E., ''Sub-Nyquist Interferometry,'' *Appl. Opt.*, 26, 5245–5258 (1987).

Hansler R. L., ''A Holographic Foucault Knife-Edge Test for Optical Elements of Arbitrary Design,'' *Appl. Opt.*, 7, 1863–1864 (1968).

Hariharan P., B. F. Oreb, and N. Brown, ''A Digital Phase-Measurement System for Real- Time Holographic Interferometry,'' *Opt. Commun.*, 41, 393–396 (1982).

Hariharan P., ''Quasi-Heterodyne Hologram Interferometry,'' *Opt. Eng.*, 24, 632–638 (1985).

Heintze L. R., H. D. Polster, and J. Vrabel, ''A Multiple-Beam Interferometer for Use with Spherical Wavefronts,'' *Appl. Opt.*, 6, 1924 (1967).

Hildebrand B. P., K. A. Haines, and R. Larkin, ''Holography as a Tool in the Testing of Large Apertures,'' *Appl. Opt.*, 6, 1267–1269 (1967a).

Hildebrand B. P. and K. A. Haines, ''Multiple-Wavelength and Multiple-Source Holography Applied to Contour Generation,'' *J. Opt. Soc. Am.*, 57, 155–162 (1967b).

Hindle J. H., ''A New Test for Cassegrainian and Gregorian Secondary Mirrors,'' *Mon. Not. R. Astron. Soc*., 91, 592 (1931).

Holleran R. T., ''Immersion Null Test for Aspherics,'' *Appl. Opt.*, 2, 1336 (1963).

Holleran R. T., ''Null Testing Telescope Mirrors by Immersion,'' *Sky Telesc.*, 28, 242 (1964).

Holleran R. T., ''Third-Order Wavefronts and Related Null Tests,'' *Appl. Opt.*, 5, 1244 (1966).

Holleran R. T., ''An Algebraic Solution for the Small Lens Null Compensator,'' *Appl. Opt.*, 7, 137 (1968).

Houston J. B., Jr., C. J. Buccini, and P. K. O'Neill, ''A Laser Unequal Path Interferometer for the Optical Shop,'' *Appl. Opt.*, 6, 1237 (1967).

Howard J. W., M. H. Beaulieu, and R. J. Zielinski, ''A Nonobscuring, Easily-Callibrated Method for Testing Ellipsoids on a Fizeau Interferometer,'' *Proc. SPIE*, 389, 26 (1983).

James W. E. and M. D. Waterworth, ''A Method for Testing Aspheric Surfaces,'' *Opt. Acta*, 12, 223–227 (1965).

Jensen S. C., W. W. Chow, and G. N. Lawrence, ''Subaperture Testing Approaches: A Comparison,'' *Appl. Opt.*, 23, 740–744 (1984).

Kirkham A. R., ''The Ronchi Test for Mirrors, '' in: *Amateur Telescope Making*, vol. 1, A. G. Ingalls, Ed., Scientific American, New York, 1953, p. 264.

Lam P., J. D. Gaskill, and J. C. Wyant, Two Wavelength Holographic Interferometer,'' *Appl. Opt.*, 23, 3079–3081 (1984).

Lamprecht J., N. Lindlein, and J. Schwider, ''Null Test Measurement of High-Numerical-Aperture Cylindrical Microlenses in Transmitted Light,'' *Proc. SPIE*, 5180, 253 (2003).

Landgrave J. E. A. and J. R. Moya, ''Dummy Lens for the Computer Optimization of Autostigmatic Null Correctors,'' *Appl. Opt.*, 26, 2673 (1987).

Lee W. H., ''Sampled Fourier Transform Hologram Generated by Computer,'' *Appl. Opt.*, 9, 639–643 (1970).

Lee W. H., ''Binary Synthetic Holograms,'' *Appl. Opt.*, 13, 1677–1682 (1974).

Leung K. M., T. C. Lee, E. Bernal G., and J. C. Wyant, ''Two-Wavelength Contouring with the Automated Thermoplastic Holographic Camera, '' *Proc. SPIE*, 192, 184–189 (1979).

Leung K. M., J. C. Lindquist, and L. T. Shepherd, ''E-Beam Computer Generated Holograms for Aspheric Testing,'' *Proc. SPIE*, 215, 70–75 (1980).

Liesener J. and H. Tiziani, ''Interferometer with Dynamic Reference,'' *Proc. SPIE*, 5252, 264–271 (2004).

Liesener J., L. Seifert, H. J. Tiziani, and W. Osten, ''Active Wavefront Sensing and Wavefront Control with SLMs,'' *Proc. SPIE*, 5532, 147–158 (2004).

Liu Y.-M., G. N. Lawrence, and C. L. Koliopoulos, ''Subaperture Testing of Aspheres with Annular Zones'' *Appl. Opt.*, 27, 4504–4513 (1988).

Loomis J. S., ''Computer-Generated Holography and Optical Testing,'' *Opt. Eng.*, 19, 679–685 (1980).

Lurionov N. P., A. V. Lukin, and K. S. Mustafin, ''Holographic Inspection of Shapes of Unpolished Surfaces,'' *Sov. J. Opt. Technol.*, 39, 154–155 (1972).

MacGovern A. J. and J. C. Wyant, ''Computer Generated Holograms for Testing Optical Elements,'' *Appl. Opt.*, 10, 619–624 (1971).

Malacara Z. and D. Malacara, ''Design of Lenses to Project the Image of a Pupil in Optical Testing Interferometers,'' *Appl. Opt.*, 34, 739–742 (1995).

Malacara D. and Menchaca, C., ''Imaging of the Wavefront Under Test in Interferometry,'' *Proc. SPIE*, 540, 34 (1985).

Meinel A. B. and M. P. Meinel, ''Self-Null Corrector Test for Telescope Hyperbolic Secondaries,'' *Appl. Opt.*, 22, 520 (1983a).

Meinel A. B. and M. P. Meinel, ''Self-Null Corrector Test for Telescope Hyperbolic Secondaries: Comments,'' *Appl. Opt.*, 22, 2405 (1983b).

Melozzi M., L. Pezzati, and A. Mazzoni, ''Testing Aspheric Surfaces Using Multiple Annular Interferograms,'' *Opt. Eng.*, 32, 1073–1079 (1993).

Mercier R., F. Bridou, B. Bonino, and M. Mullot, ''Control of Aspherics by In-Line Computer-Generated Holograms,'' *Proc. SPIE*, 235, 80–84 (1980).

Moya J. R. and J. E. A. Landgrave, ''Third-Order Design of Refractive Offner Compensators,'' *Appl. Opt.*, 26, 2667 (1987).

Negro J. E., ''Subaperture Optical System Testing,'' *Appl. Opt.*, 23, 1921–1930 (1984).

Norman B. A., ''New Test for Cassegrainian Secondaries,'' *Sky Telesc.*, 17, 38 (1957).

Offner A., ''A Null Corrector for Paraboloidal Mirrors,'' *Appl. Opt.*, 2, 153 (1963).

Offner A., ''Field Lenses and Secondary Axial Aberration,'' *Appl. Opt.*, 8, 1735 (1969).

Ono A. and J. C. Wyant, ''Plotting Errors Measurement of CGH Using an Improved Interferometric Method,'' *Appl. Opt.*, 23, 3905–3910 (1984).

Parks R. E., ''Making and Testing an f/0.15 Parabola,'' *Appl. Opt.*, 13, 1987–1987 (1974).

Parks R. E. and L. Z. Shao, ''Testing Large Hyperbolic Secondary Mirrors,'' *Opt. Eng.*, 27, 1057 (1988).

Pastor J., ''Hologram Interferometry and Optical Technology,'' *Appl. Opt.*, 8, 525–531 (1969).

Pruss C., S. Reichelt, H. J. Tiziani, and W. Osten, ''Computer-Generated Holograms in Interferometric Testing,'' *Opt. Eng.*, 43, 2534–2540 (2004).

Puryayev D. T., ''A Quality Control Technique *for* Convex Elliptical, Parabolic and Hyperbolic Surfaces of Simple Lenses,'' *Soc. J. Opt. Technol.*, 38, 684 (1971).

Puryayev D. T., ''Compensator for Inspecting the Quality of Large-Diameter Parabolic Mirrors,'' *Sov. J. Opt. Technol.*, 40, 238 (1973).

Reichelt S., C. Pruss, and H. J. Tiziani, ''Absolute Testing of Aspheric Surfaces,'' *Proc. SPIE*, 5252, 252–263 (2004).

Ritchey G. W., ''On the Modern Reflecting Telescope and the Making and Testing of Optical Mirrors,'' *Smithson. Contrib. Knowl*., 34, 3 (1904).

Robbert C. F., ''Typical Error Budget for Testing High-Performance Aspheric Telescope Mirror,'' *Proc. SPIE*, 181, 56 (1979).

Rodgers J. M. and R. E. Parks, ''Null Tests for Oblate Spheroids,'' *Appl. Opt.*, 23, 1246–1247 (1984).

Rodgers J. M., ''A Null-Lens Design Approach for Centrally Obscured Components,'' *Proc. SPIE*, 679, 17 (1986).

Ross F. E., ''Parabolizing Mirrors without a Flat,'' *Astrophys. J.*, 98, 341 (1943).

Sasian J. M., ''Design of Null Correctors for the Testing of Astronomical Optics,'' *Opt. Eng*., 27, 1051 (1988).

Sasian J. M., ''Optimum Configuration of the Offner Null Corrector: Testing an F/1 Paraboloid,'' *Proc. SPIE*, 1164, 8 (1989).

Schlauch J., ''Construction of a Dall Null Tester,'' *Sky Telesc.*, 18, 222 (1959).

Schupmann L., *Die Medial-Fernrohre:* Eine *neue Konstruktion jar grosse astronomische Inhrumente*, Teubner, Leipzig, 1899.

Schwider J. and R. Burow, ''The Testing of Aspherics by Means of Rotational-Symmetric Synthetic Holograms,'' *Opt. Appl*., 6, 83 (1976).

Schwider J., ''Interferometric Tests for Aspherics,'' *OSA TOPS*, 24, 103–114 (1999).

Shafer D. R., ''Zoom Null Lens,'' *Appl. Opt.*, 18, 3863 (1979).

Shnurr A. D. and A. Mann, ''Optical Figure Characterization for Cylindrical Mirrors and Lenses,'' *Opt. Eng*., 20, 412–416 (1981).

Silvertooth W., ''A Modification of the Hindle Test for Cassegrain Secondaries,'' *J. Opt. Soc Am.*, 30, 140 (1940).

Simpson F. A., B. H. Oland, and J. Meckel, ''Testing Convex Aspheric Lens Surfaces with a Modified Hindle Arrangement,'' *Opt. Eng*., 13, 101 (1974).

Sjödahl M. and B. F. Oreb, ''Stitching Interferometric Measurement Data for Inspection of Large Optical Components,'' *Opt. Eng.*, 41, 403–408 (2002).

Snow K. and R. Vandewarker, ''On Using Holograms for Test Glasses,'' *Appl. Opt.*, 9, 822–827 (1970).

Stoltzmann D. E. and M. Hatch, ''Extensions of the Dall Null Test,'' *Sky Telesc.*, 52, 210 (1976).

Tiziani H. J., S. Reichlet, C. Pruss, M. Rocktächel, and U. Hofbauer, ''Testing of Aspheric Surfaces,'' *Proc. SPIE*, 4440, 109–119 (2001).

Uhrich C. and L. Hesselink, ''Optical Surface Inspection Using Real-Time Fourier Transform Holography in Photorefractives,'' *Appl. Opt.*, 27, 4497–4503 (1988).

Wyant J. C., ''Testing Aspherics Using Two-Wavelength Holography,'' *Appl. Opt.*, 10, 2113–2118 (1971).

Wyant J. C. and K. Creath, ''Two-Wavelength Phase-Shifting Interferometer and Method,'' U.S. Patent No. 4,832,489 (1989).

Wyant J. C. and V. P. Bennett, ''Using Computer Generated Holograms to Test Aspheric Wavefronts,'' *Appl. Opt.*, 11, 2833–2839 (1972).

Wyant J. C. and P. K. O'Neill, ''Computer Generated Hologram: Null Lens Test of Aspheric Wavefronts,'' *Appl. Opt.*, 13, 2762–2765 (1974).

Wyant J. C., B. F. Oreb, and P. Hariharan, ''Testing Aspherics Using Two-Wavelength Holography: Use of Digital Electronic Techniques,'' *Appl. Opt.*, 23, 4020–4023 (1984).

Author Query

Q1. Author Please check the change made in year.
Q2. Author Please check.
Q3. Author Please check.
Q4. Author Please check whether the a or b.
Q5. Author Please check the change made in date.
Q6. Author Please check the change made in figure citation.